

Document downloaded from:

<http://hdl.handle.net/10251/122228>

This paper must be cited as:

Sorribes, I.; Liu, L.; Doménech Carbó, A.; Corma Canós, A. (2018). Nanolayered Cobalt-Molybdenum Sulfides as Highly Chemo- and Regioselective Catalysts for the Hydrogenation of Quinoline Derivatives. *ACS Catalysis*. 8(5):4545-4557.

<https://doi.org/10.1021/acscatal.7b04260>



The final publication is available at

<http://doi.org/10.1021/acscatal.7b04260>

Copyright American Chemical Society

Additional Information

# Nanolayered Cobalt-Molybdenum Sulfides as Highly Chemo- and Regioselective Catalysts for the Hydrogenation of Quinoline Derivatives

*Iván Sorribes,<sup>†</sup> Lichen Liu,<sup>†</sup> Antonio Doménech-Carbó,<sup>‡</sup> and Avelino Corma<sup>\*†</sup>*

<sup>†</sup>Instituto de Tecnología Química, Universitat Politècnica de València-Consejo Superior de Investigaciones Científicas, Avenida de los Naranjos s/n, 46022 Valencia, Spain.

<sup>‡</sup>Departament de Química Analítica. Universitat de València, Dr. Moliner, 50, 46100 Burjassot (Valencia), Spain.

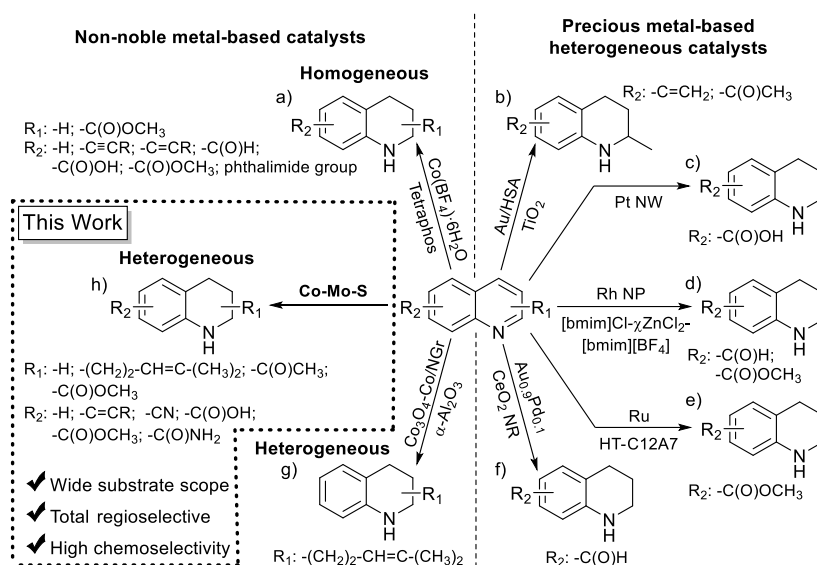
**ABSTRACT:** Herein, a general protocol for the preparation of a broad range of valuable *N*-heterocyclic products by hydrogenation of quinolines and related *N*-heteroarenes is described. Interestingly, the catalytic hydrogenation of the *N*-heteroarene ring is chemoselectively performed when other facile reducible functional groups, including alkenes, ketones, cyanides, carboxylic acids, esters and amides, are present. The key to successful catalysis relies on the use of a nanolayered cobalt-molybdenum sulfide catalyst hydrothermally synthesized from earth abundant metal precursors. This heterogeneous system displays a tunable composition of phases that allows for catalyst regeneration. Its catalytic activity depends on the composition of the mixed phase of cobalt sulfides, being higher with the presence of Co<sub>3</sub>S<sub>4</sub>, and could also be associated to the presence of transient Co-Mo-S structures that are mainly vanished after the first catalytic run.

**KEYWORDS:** Chemo-/Regioselective hydrogenation, Heterogeneous catalysis, Quinolines, *N*-heterocycles, Co-Mo-S catalysts

## INTRODUCTION

Catalytic hydrogenation of *N*-heteroarenes is a fundamentally important reaction in the petrochemical industry and represents a promising method for organic synthesis.<sup>1,2</sup> In particular, the hydrogenation of quinoline derivatives has drawn the attention of the synthetic chemists because of its practical simplicity and high atom efficiency for the production of 1,2,3,4-tetrahydroquinolines, a core structural motif present in many alkaloids and bioactive molecules used as drugs and agrochemicals.<sup>3</sup> However, hydrogenation of these *N*-heteroarenes involves the challenging tasks of breaking aromaticity as well as overcoming catalyst poisoning by strong interaction with starting materials and their hydrogenated products.<sup>2c,4</sup> Nonetheless, different homogeneous systems based on transition metals, such as Ir,<sup>5</sup> Ru,<sup>5a,6</sup> Rh,<sup>5a,7</sup> Mo,<sup>8</sup> Os,<sup>5a,9</sup> Fe<sup>10</sup> and Co<sup>11</sup>, have been applied for the hydrogenation of quinolines. Particularly worth mentioning since it represents a suitable route to valuable *N*-heterocyclic compounds, is a well-defined homogeneous cobalt catalyst that allows the chemoselective hydrogenation of *N*-heteroarenes functionalized with other sensitive reducible groups (Scheme 1a).<sup>11b,12</sup> However, despite the good reactivity and selectivity exhibited by some of these homogeneous catalysts, the use of air-sensitive and/or expensive ligands, additives as well as the inherent recyclability issues hinder their industrial scale application. In contrast, heterogeneous catalytic systems offer a convenient alternative since catalysts can be easily recovered and reused. Different heterogeneous catalysts based on precious metals including Pd,<sup>13</sup> Pt,<sup>14</sup> Rh,<sup>14a,15</sup> Ru,<sup>16</sup> Ir<sup>14a,17</sup> or Au<sup>13h,18</sup> have been used for the hydrogenation of quinolines and its derivatives. In general, they are highly active but are not selective displaying low functional group tolerance. In fact, only a handful of

these precious metal-based heterogeneous catalysts allow for the chemoselective hydrogenation of quinolines in the presence of other reducible functionalities.



**Scheme 1.** Chemoselective hydrogenation of quinolines bearing other reducible functional groups

In 2012, Cao and co-workers<sup>18</sup> described that Au nanoparticles supported on high surface area (HSA) TiO<sub>2</sub> can selectively hydrogenate the *N*-heteroarene ring of quinolines bearing olefinic and ketone groups (Scheme 1b).<sup>18-19</sup> In 2013, the chemoselectivity was expanded to the presence of a carboxylic acid group using a Pt nanowire-type catalyst (Scheme 1c).<sup>14b</sup> More recently, Rh nanoparticles immobilized in a Lewis acid ionic liquid,<sup>15i</sup> as well as Ru and bimetallic AuPd nanoparticles supported on nanoporous 12CaO·7Al<sub>2</sub>O<sub>3</sub><sup>16k</sup> or CeO<sub>2</sub> nanorods,<sup>13h</sup> respectively, have also been applied for the preparation of 1,2,3,4-tetrahydroquinolines functionalized with aldehydes or esters groups by hydrogenation of their parent quinolines (Scheme 1d-f). Despite their selectivity, it is today an important issue to replace precious metals by earth-abundant metal-based catalysts, and this is also the case for the hydrogenation of *N*-heteroarenes.

Nowadays, heterogeneous approaches using non-noble metals for the synthesis of 1,2,3,4-tetrahydroquinolines by hydrogenation of quinolines are scarce. They involve the use of traditional Raney®-Ni<sup>2b,20</sup> or cobalt-based catalysts.<sup>21</sup> In addition, these catalytic systems present a limited substrate scope, especially for quinolines functionalized with other reducible functional groups. A catalyst based on *N*-graphene-modified cobalt nanoparticles supported on alumina, was applied for the chemoselective hydrogenation of a quinoline bearing an olefinic group (Scheme 1g).<sup>21a,22</sup> However, this selectivity was only demonstrated at moderate conversion (61%), reached after long reaction time (48 h). Furthermore, the selectivity when other functional groups were present was not reported. Hence, heterogeneous catalysts based on non-noble metals with superior activity and chemoselectivity for quinolines hydrogenation are still highly desirable.

Herein, we describe the hydrothermal preparation of nanolayered mixed cobalt-molybdenum sulfide (Co-Mo-S) materials. We demonstrate that their application as catalysts for quinolines hydrogenation allows for the straightforward and general preparation of 1,2,3,4-tetrahydroquinolines with high tolerance to other sensitive moieties (Scheme 1h). Furthermore, we show that the non-noble metal-based catalytic system presented here is also applicable for the regioselective hydrogenation of other heteroaromatic nitrogen compounds.

## RESULTS AND DISCUSSION

### Preparation and Characterization of Catalysts

Hydrogenation of the heteroaromatic ring of *N*-heteroarene compounds constitutes a key step of the overall reaction schemes involved in the hydrodenitrogenation (HDN) processes, routinely applied in petroleum refineries for removing nitrogen heteroatoms from crude feed-stocks.<sup>23</sup> Promoted molybdenum sulfides, specifically by nickel, are the

most commonly used catalysts for HDN processes, while molybdenum disulfide cobalt-promoted materials are more widespread used for hydrodesulfurization (HDS).<sup>1,24</sup> It is well-established that in these materials the Co-Mo-S (or Ni-Mo-S) structures, formed by adsorption of cobalt (or Ni) on the edge positions of MoS<sub>2</sub> layers, plays a crucial role in their catalytic activity.<sup>25,26</sup> Recently, Mavrikakis and co-workers using density functional theory (DFT) have shown that nitrogen-containing compounds, including quinolines, tend to be strongly adsorbed and activated on the “brim” sites of the Co-Mo-S structure edges due to the presence of metal-like electronic states.<sup>25k,25n,27</sup> This background suggests that cobalt-molybdenum sulfide-based catalysts could also be of interest for the efficient hydrogenation of *N*-heteroarenes. Nevertheless, so far, there are not general catalytic protocols for the hydrogenation of quinolines to 1,2,3,4-tetrahydroquinolines by using these type of catalysts.<sup>24a,28</sup>

Quite recently, we reported the hydrothermal preparation of nanolayered molybdenum disulfide cobalt-promoted materials and their application as catalysts for the chemoselective hydrogenation of nitroarenes.<sup>29</sup> All prepared Co-Mo-S-X catalysts contained, as determined by ICP analysis, either lower or the same cobalt content with respect to molybdenum ( $X = \text{Co}/(\text{Mo} + \text{Co})$  mole ratio  $\leq 0.5$ ). In contrast, in the present work we have adapted this synthetic methodology to obtain Co-Mo-S-X unsupported materials in which the content of cobalt is higher than that molybdenum ( $X = \text{Co}/(\text{Mo} + \text{Co})$  mole ratio  $> 0.5$ ). In this way, the preparation was performed at 180 °C in an autoclave containing ammonium molybdate, sulfur, different amounts of cobalt(II) acetate, and an aqueous solution of hydrazine. In addition, the catalyst Co-Mo-S-0.39 that contains more molybdenum than cobalt, molybdenum disulfide and two different molybdenum-free cobalt sulfide materials were also prepared (see reference 29 and the Supporting Information for characterization and preparation details). It should be noted

that the catalyst Co-Mo-S-0.39 displayed high activity and selectivity for the chemoselective hydrogenation of nitroarenes.<sup>29</sup>

X-ray diffraction (XRD) patterns of the prepared materials with different cobalt content are shown in Figure 1. All of them are dominated by the presence of diffraction peaks associated to cobalt sulfide species. Catalysts Co-Mo-S-0.58 and Co-Mo-S-0.66 exhibit similar diffraction patterns with peaks at  $2\theta$  values of  $28^\circ$ ,  $32^\circ$ ,  $36^\circ$ ,  $40^\circ$ ,  $46^\circ$ ,  $55^\circ$ ,  $58^\circ$ ,  $60^\circ$ ,  $63^\circ$ ,  $75^\circ$ ,  $77^\circ$ ,  $79^\circ$ ,  $86^\circ$  corresponding to the (111), (200), (210), (211), (220), (311), (222), (230), (321), (331), (420), (421) and (422) planes of  $\text{CoS}_2$  (PDF Card 00-041-1471). Notably, most of these peaks are very sharp, indicating that  $\text{CoS}_2$  is present in the form of large particles. In addition, the broad diffraction peaks at  $14^\circ$ ,  $33^\circ$ ,  $39^\circ$ ,  $58^\circ$  characteristic of the (002), (101), (103) and (110) basal planes of  $\text{MoS}_2$  with very low crystallinity can also be detected. When a higher amount of the cobalt salt was used in the catalyst preparation, the obtained material Co-Mo-S-0.83 is constituted by different cobalt sulfide phases. Together with a significant decrease of  $\text{CoS}_2$  diffraction peaks, the XRD pattern shows the presence of peaks at  $2\theta$  values of  $32^\circ$ ,  $38^\circ$ ,  $47^\circ$ ,  $50^\circ$ ,  $55^\circ$  which can be indexed to the (311), (400), (422), (333) and (440) planes of the cubic phase of  $\text{Co}_3\text{S}_4$  (PDF card 00-011-0121). These XRD peaks are much broader than those of  $\text{CoS}_2$  in catalysts Co-Mo-S-0.58 and Co-Mo-S-0.66, indicating that the surface area of the  $\text{Co}_3\text{S}_4$  phase is larger than that of  $\text{CoS}_2$ . Further increase of the initial cobalt salt amount leads to the formation of the  $\text{Co}_9\text{S}_8$  phase in the material Co-Mo-S-0.91. It should be noted that the increase of Co content also affects the crystalline structure of the  $\text{MoS}_2$  phase. By comparing the XRD patterns in Figure 1, it can be seen that the intensity of the diffraction peak associated to the (002) plane, that is representative for the stacking of  $\text{MoS}_2$  layers, undergoes a significant decrease in materials Co-Mo-S-0.83 and Co-Mo-S-0.91, thus revealing that  $\text{MoS}_2$  is present with a limited number of

stacked atomic layers. In all prepared catalysts, XRD peaks of the ternary Co-Mo-S structure are indistinguishable from those of MoS<sub>2</sub> because the Co-Mo-S structure consists of MoS<sub>2</sub> decorated at the edges by cobalt atoms. Therefore, the XRD is totally determined by the MoS<sub>2</sub> part.<sup>30</sup>

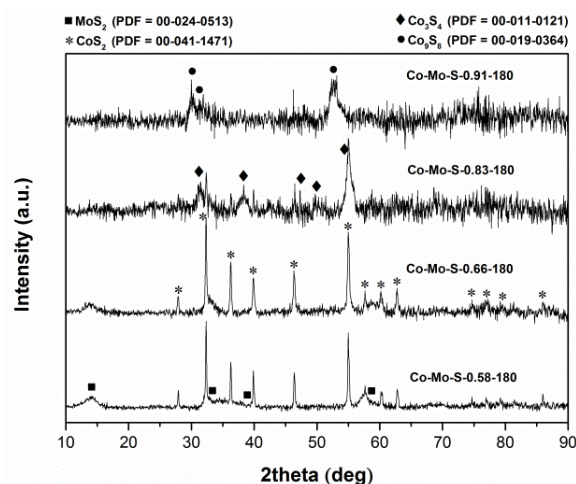


**Figure 1.** X-ray diffraction patterns of mixed cobalt-molybdenum sulfide (Co-Mo-S) catalysts

Microstructure details of prepared Co-Mo-S catalysts were analyzed by high-resolution transmission electron microscopy (HRTEM) and the results are shown in Figure 2. Catalysts Co-Mo-S-0.58 and Co-Mo-S-0.66 exhibit the characteristic group of parallel fringes with an average number of stacked layers of 5-8 and with an interlayer distance of 0.63-0.64 nm, which correspond to the (002) plane of MoS<sub>2</sub> (Figure 2a-d).<sup>31</sup> Free CoS<sub>2</sub> particles of different sizes (Table S1 in the Supporting Information), that displays the characteristic lattice-fringes spacing of 0.27 and 0.25 nm, associated with the (200) and (210) planes respectively, are widely found in both catalysts. However, catalyst Co-Mo-S-0.66 displays more interlaced MoS<sub>2</sub> and CoS<sub>2</sub> phases assuring the strong interaction between them, and thus promoting a presumably higher formation of active Co-Mo-S structures. This is consistent with the metal distributions determined by Energy-dispersive X-ray (EDX) elemental mapping (Figures S1-S2 in the Supporting



Information). HRTEM micrographs of catalyst Co-Mo-S-0.83 display the three obviously different lattice fringes with spacing of 0.63-0.64, 0.27 and 0.24 nm corresponding to (002), (200) and (400) planes of MoS<sub>2</sub>, CoS<sub>2</sub> and Co<sub>3</sub>S<sub>4</sub>, respectively (Figure 2e-g). In contrast, the interlayer distances of 0.30 and 0.25 nm characteristic of (311) and (400) planes of Co<sub>9</sub>S<sub>8</sub> phase are detected in catalyst Co-Mo-S-0.91 (Figure 2h). Notably, MoS<sub>2</sub> is hardly found as isolated layers, which is in concordance with the XRD analysis that revealed a depressed layer stacking with the increase of cobalt content. Component distributions of catalysts Co-Mo-S-0.83 and Co-Mo-S-0.91 were determined by EDX elemental mapping revealing that these materials are mostly constituted by cobalt and sulfur with low content of molybdenum but homogeneously distributed on cobalt sulfide phases (Figure 3 and Figure S3 in the Supporting Information).

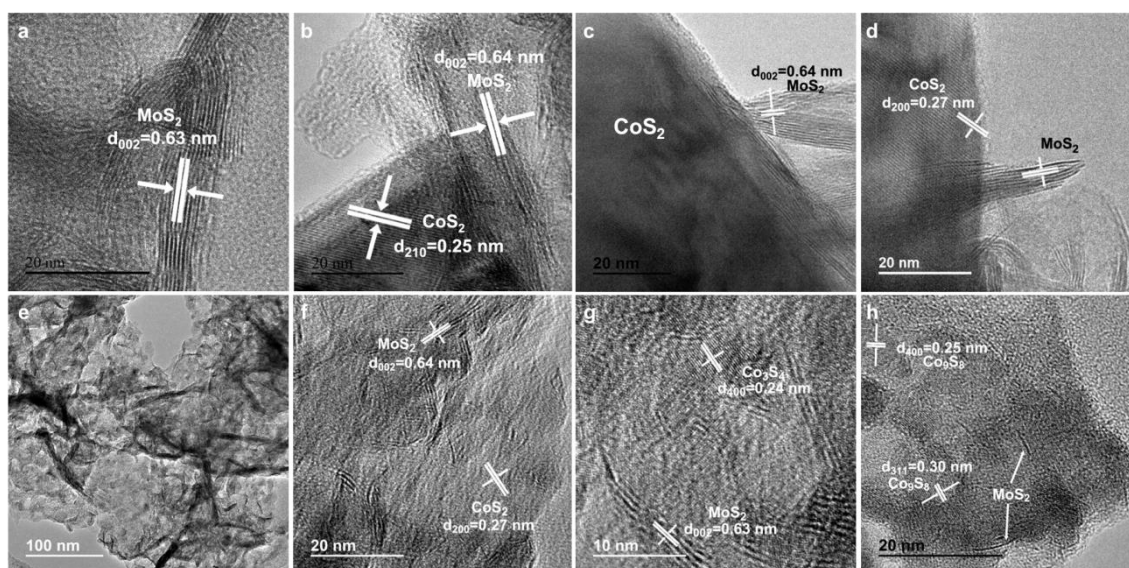


**Figure 2.** HRTEM micrographs of (a,b) Co-Mo-S-0.58, (c,d) Co-Mo-S-0.66, (e-g) Co-Mo-S-0.83, (h) Co-Mo-S-0.91

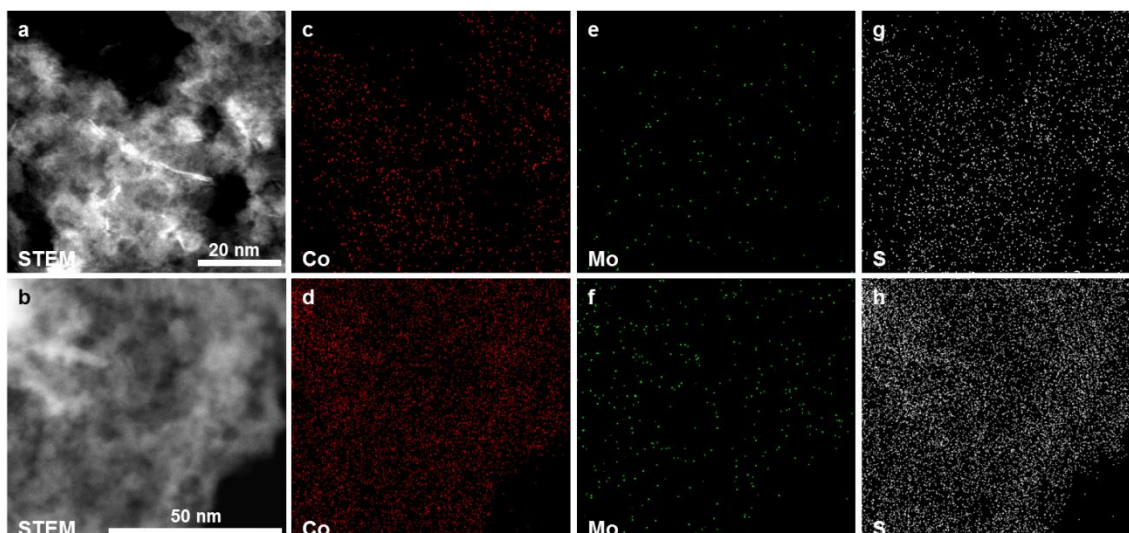


**Figure 3.** (a,b) High-angle annular dark-field scanning transmission electron microscopy (HAADF-STEM) images of Co-Mo-S-0.83. (c-h) EDX elemental mapping of cobalt, molybdenum and sulfur

Further characterization of catalysts was carried out by nitrogen physisorption studies. The specific surfaces areas (SA), total pore volumes (PV) and pore size (PS) of catalysts containing different Co/(Mo + Co) mole ratios are summarized in Table 1. The SA and PV range from 80 to 44 m<sup>2</sup>/g and 0.18 to 0.07 cm<sup>3</sup>/g, respectively. Catalyst Co-Mo-S-0.58 presents the highest values, but a progressive decrease in both SA and PV is achieved upon increasing the Co/(Mo + Co) mole ratio. This decrease can be attributed to the lower MoS<sub>2</sub> content and the concomitant formation of cobalt sulfide phases with lower surface area but higher pore size.

**Table 1.** BET surface area, pore volume and pore diameter of Co-Mo-S catalysts

Catalyst	Surface Area (m <sup>2</sup> /g)	Pore Volume (cm <sup>3</sup> /g)	Pore Diameter (nm)
Co-Mo-S-0.58-180	79.4	0.18	9.2
Co-Mo-S-0.66-180	63.4	0.15	9.6
Co-Mo-S-0.83-180	48.9	0.07	10.3
Co-Mo-S-0.91-180	44.4	0.08	13.2

## Catalytic Results

The hydrogenation of quinoline (**1a**) to the corresponding 1,2,3,4-tetrahydroquinoline (**2a**) was investigated as the benchmark system to compare the catalytic activity of the prepared cobalt-molybdenum sulfide materials. Initial hydrogenation experiments were performed in a batch reactor using toluene as solvent, under 12 bar of H<sub>2</sub>, at 150 °C and 1000 rpm of stirring speed to avoid limitation by external diffusion (Figure S6 in the Supporting Information). As shown in Figure 4, the catalyst Co-Mo-S-0.83, mainly constituted by a mixture of MoS<sub>2</sub>, CoS<sub>2</sub> and Co<sub>3</sub>S<sub>4</sub> phases, proved to be the most active system achieving after 6 h almost full conversion of **1a** with excellent regioselectivity to the desired hydrogenated product **2a**. In the presence of catalyst Co-Mo-S-0.91, which contains a different cobalt sulfide phase of Co<sub>9</sub>S<sub>8</sub>, **1a** undergoes lower conversion, thus revealing that the cobalt phase composition of the catalyst exerts a significant effect on its catalytic performance. Different activity is also observed for catalysts Co-Mo-S-0.39, Co-Mo-S-0.58 and Co-Mo-S-0.66, all of them formed by MoS<sub>2</sub> and CoS<sub>2</sub> as major phases. Apart from their different metal mole ratio, these catalysts present significant differences on the metal distribution, as it has been inferred by electron microscopy characterization (Figure 2, Figures S1-S2 in the Supporting Information and reference 29). Catalyst Co-Mo-S-0.58, with more separated CoS<sub>2</sub> phase, displays the lowest catalytic activity. However, conversion of **1a** is enhanced in catalysts Co-Mo-S-0.39 and Co-Mo-S-0.66 with metal sulfides more homogeneously distributed, as a result of the generation of Co-Mo-S active structures to a larger extent.<sup>25</sup> It is noteworthy that the use of MoS<sub>2</sub> or cobalt sulfides as catalysts leads to lower conversions of **1a** than all prepared Co-Mo-S catalysts. Nevertheless, an excellent regioselectivity of the *N*-heteroarene ring hydrogenation is achieved in all prepared materials with no detection of reaction intermediates or over-hydrogenated products (Figure S7 in the Supporting

Information). As in the case of the so-called Nebula catalyst,<sup>24e,32</sup> comparison of the catalytic activity per unit volume of catalyst between these unsupported Co-Mo-S catalysts and a conventional supported one reveals that our prepared unsupported catalysts display a larger population of active sites per unit volume (Figure S8 in the Supporting Information). Thus, despite of their higher cost, they allow for a higher throughput.

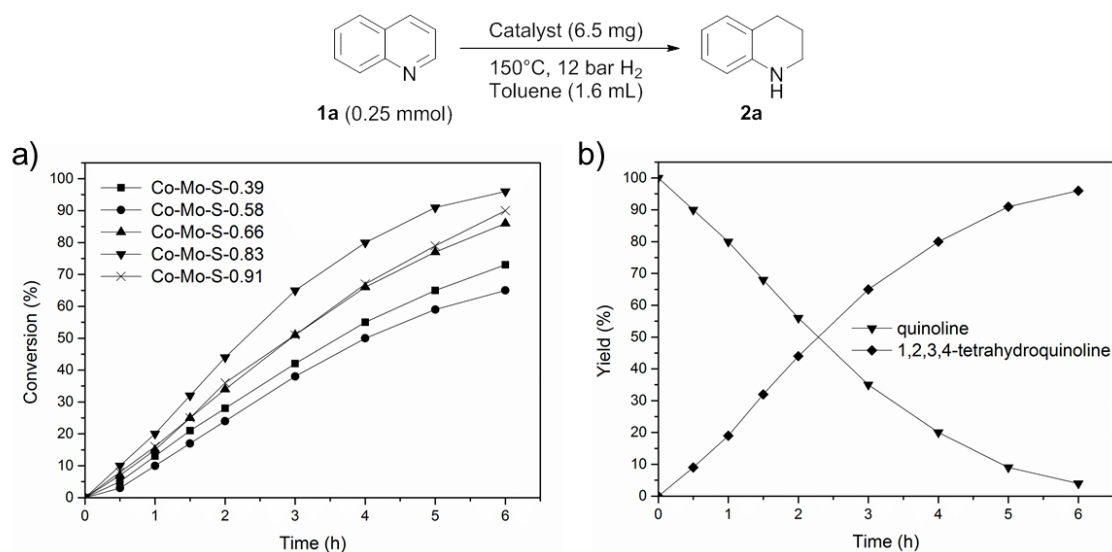
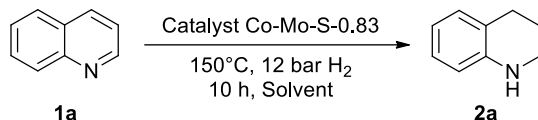


**Figure 4.** (a) Catalytic performance of Co-Mo-S catalysts for the hydrogenation of quinoline (**1a**) to 1,2,3,4-tetrahydroquinoline (**2a**). (b) Yield of **1a** and **2a** versus reaction time for catalyst Co-Mo-S-0.83.

Further optimization experiments were carried out with the most active catalyst (Co-Mo-S-0.83). First, the influence of the solvent was investigated (Table 2, entries 1-8). In general, the use of other solvents different than toluene led to lower reactivity. At longer reaction time (10 h), excellent conversions of **1a** were also achieved by using protic solvents, such as ethanol and methanol (Table 2, entries 1-2). Interestingly, in the absence of any solvent **2a** is obtained in excellent yield in 2h (Table 2, entry 8). The catalytic hydrogenation of **1a** could also be achieved at lower temperature affording **2a** in a quantitative yield at 120 °C or 87% yield at 100 °C with after longer reaction time

(Table 2, entries 9 and 10). When hydrogen pressure was halved, **1a** was almost fully converted affording **2a** in 90% yield (Table 2, entry 11).

**Table 2.** Regioselective hydrogenation of quinoline (**1a**) catalyzed by Co-Mo-S-0.83<sup>a</sup>



Entry	Solvent	Conversion (%) <sup>b</sup>	Yield (%) <sup>b</sup>
1	EtOH	94	91
2	MeOH	84	83
3	1,4-dioxane	60	50
4	CH <sub>3</sub> CN	20	14
5	THF	21	11
6	<i>n</i> -Bu <sub>2</sub> O	67	58
7	Toluene	>99	98
8 <sup>c</sup>	-	99	98 <sup>d</sup>
9 <sup>e</sup>	Toluene	99	99 (92)
10 <sup>f</sup>	Toluene	87	87
11 <sup>g</sup>	Toluene	92	90

<sup>a</sup>Reaction conditions: **1a** (0.25 mmol), catalyst (6.5 mg), solvent (1.6 mL). <sup>b</sup>Determined by GC using dodecane as an internal standard; yield of isolated product on a 10 mmol scale in parentheses. <sup>c</sup>2 h. <sup>d</sup>Average value for 6 catalytic reactions: (97.8 ± 1.1). <sup>e</sup>120 °C, 12 h. <sup>f</sup>100 °C, 18 h. <sup>g</sup>120 °C, 12 h, 6 bar H<sub>2</sub>.

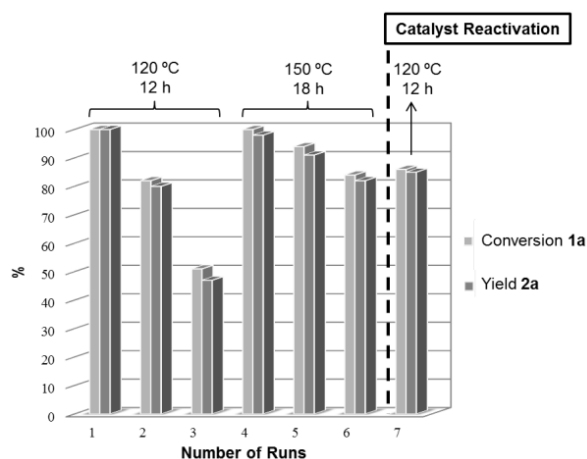


**Figure 5.** Catalyst recycling for the hydrogenation of quinoline (**1a**) to 1,2,3,4-tetrahydroquinoline (**2a**) before and after reactivation

With the above optimized conditions in hand (Table 2, entry 9), the stability and recyclability of catalyst Co-Mo-S-0.83 was investigated. As shown in Figure 5, the conversion of **1a** decreased gradually with the reaction cycles, being halved for the third run. Nevertheless, excellent yields of the hydrogenated product **2a** could be obtained again even after the sixth run by increasing reaction temperature (up to 150 °C) and reaction times.

XRD and HRTEM characterization of the catalyst after different catalytic cycles revealed a continuing evolution of the mixed phase of cobalt sulfides (Figures 6 and 7; see also Figures S9-S12 in the Supporting information). In the fresh catalyst, both CoS<sub>2</sub> and Co<sub>3</sub>S<sub>4</sub> are present (see Figures 1 and 2). After the first run, the Co<sub>3</sub>S<sub>4</sub> phase is present in catalyst Co-Mo-S-0.83-R1 in a higher extent as result of the transformation of some CoS<sub>2</sub>. With two additional reaction cycles, a new phase of Co<sub>9</sub>S<sub>8</sub> can also be detected in the reused catalyst Co-Mo-S-0.83-R3 indicating that the mixed phase of cobalt sulfides is further transformed. After the sixth run, the mixed phase of cobalt sulfides in catalyst Co-Mo-S-0.83-R6 is mainly constituted by Co<sub>9</sub>S<sub>8</sub>. These results and the presence of H<sub>2</sub>S in the gas-phase (detected by GC) after catalytic reaction suggest that catalyst undergoes desulfurization during the catalytic hydrogenation process. The extent of stability of the cobalt sulfide phases is in line with the previously reported thermodynamic data that predict poor stability of the CoS<sub>2</sub> and Co<sub>3</sub>S<sub>4</sub> phases under pure hydrogen atmosphere (or low content of H<sub>2</sub>S) at the working reaction temperatures.<sup>33</sup> However, while the hydrogenation of **1a** was poisoned with the presence of H<sub>2</sub>S in feed, the addition of sulfur to the reaction mixture slowed down but did not avoid the catalyst deactivation (see Figure S13 in the Supporting Information).

Interestingly, the hydrothermal treatment of the reused catalyst Co-Mo-S-0.83-R6 with an excess of sulfur powder in the presence of an aqueous solution of hydrazine

allowed the successful catalyst re-sulfurization and the recovering of most of the activity (see the Supporting Information for further details). This process leads to a new phase transformation affording a reactivated catalyst (Co-Mo-S-0.83-React) mainly formed by  $\text{Co}_3\text{S}_4$  and  $\text{CoS}_2$  as mixed phase of cobalt sulfides. This reactivated catalyst shows a similar diffraction pattern to the catalyst after one catalytic cycle (Co-Mo-S-0.83-R1), and both catalysts (Co-Mo-S-0.83-React and Co-Mo-S-0.83-R1) display similar catalytic activity for the hydrogenation of **1a** under otherwise the same reaction conditions (Figure 5). These results demonstrate that catalytic activity of this cobalt-molybdenum sulfide material relies on the cobalt phase composition, being higher with the presence of  $\text{Co}_3\text{S}_4$  phase but lower when increasing the relative content of  $\text{Co}_9\text{S}_8$  phase. Accordingly to the comparative catalytic study (see Figure 4 and Figure S7 in the Supporting Information), catalytic performance of Co-Mo-S catalysts is diminished when increasing the relative content of the separated  $\text{CoS}_2$  phase, and therefore the high activity of catalyst Co-Mo-S-0.83 could be associated to the presence of the active  $\text{Co}_3\text{S}_4$  phase. However, the reused catalyst Co-Mo-S-0.83-R1 containing  $\text{Co}_3\text{S}_4$  phase in a higher extent is less active than the fresh catalyst (Co-Mo-S-0.83), and therefore the catalytic activity should not be only ascribed to this active phase.

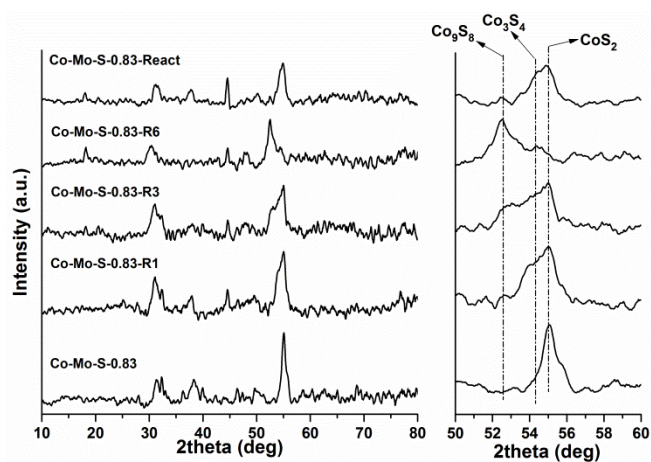


**Figure 6.** XRD patterns of reused and reactivated Co-Mo-S catalysts

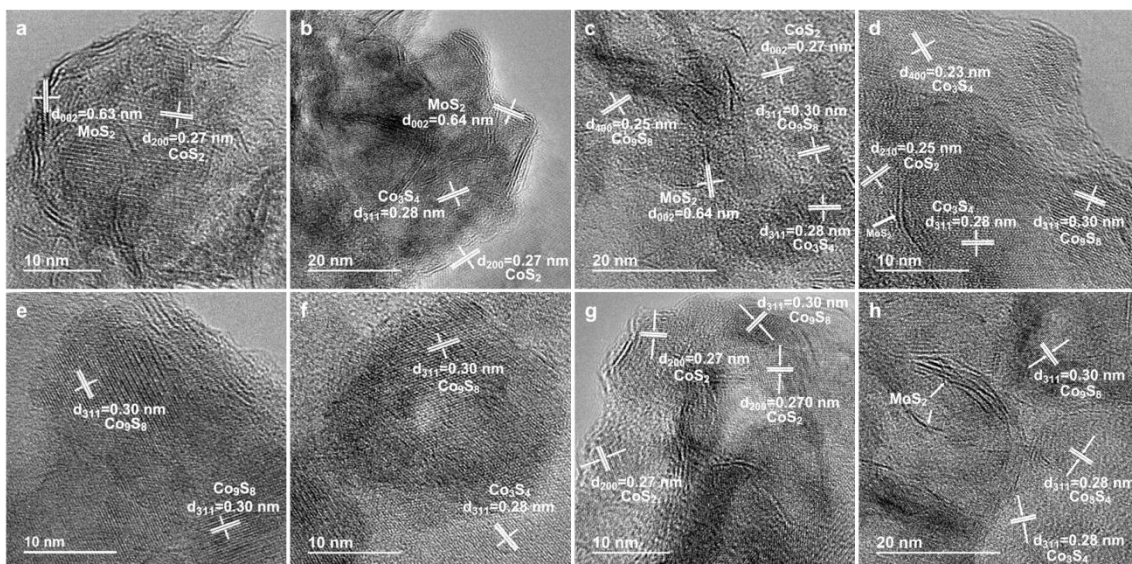


**Figure 7.** HRTEM micrographs of (a,b) Co-Mo-S-0.83-R1, (c,d) Co-Mo-S-0.83-R3, (e,f) Co-Mo-S-0.83-R6, (g,h) Co-Mo-S-0.83-React

To get more clues on the origin of the catalytic activity and therefore on the catalyst deactivation, an electrochemical study of the fresh, reused and reactivated catalysts was performed applying the voltammetry of immobilized particles (VIMP) methodology. This technique, developed by Scholz *et al.*<sup>34</sup> have provided valuable analytical information on a variety of sparingly soluble solids upon their attachment as micro- or submicrosamples to inert electrodes in contact with suitable electrolytes.<sup>35</sup> The cyclic voltammogram of the fresh catalyst Co-Mo-S-0.83 displays cathodic signals (C<sub>1</sub>) between 0.0 and -0.5 V (*vs* Ag/AgCl), preceding the prominent current peak associated to the hydrogen evolution reaction (HER),<sup>36</sup> and a main anodic signal (A<sub>1</sub>) at +0.95 V (Figure S14 in the Supporting Information). These signals can be attributed to proton-assisted solid-state reduction and sulfide-centered oxidation processes, respectively. Reused catalysts show similar cyclic voltammograms, but significant differences could be detected using a particularly sensitive technique, such as the square wave voltammetry. As shown in Figure 8A, the signal A<sub>1</sub> for the fresh catalyst presents



significant peak splitting with components at +1.02, +0.92 and +0.72 V preceding a weak peak at +1.2 V, this last one being associated to the oxidation of MoS<sub>2</sub> and CoS<sub>2</sub> (Figure S15 in the Supporting Information). However, in the cyclic voltammograms of the reused catalysts only the central component at +0.92 V of the split signal is apparently retained whereas the components at +1.02 and +0.72 V have entirely or almost vanished. Unfortunately, no clear reappearance of these last two signals is achieved under the hydrothermal regeneration process. These results indicate that both signals correspond to active species that are consumed during the catalytic cycles, mainly in the first run, being likely associated to transient Co-Mo-S structures.

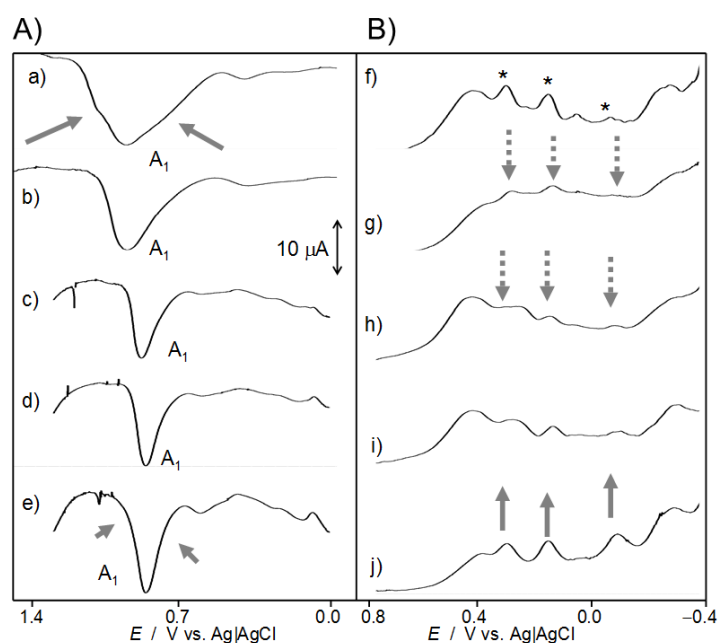


**Figure 8.** Square wave voltammograms of (a,f) Co-Mo-S-0.83, (b,g) Co-Mo-S-0.83-R1, (c,h) Co-Mo-S-0.83-R3, (d,i) Co-Mo-S-0.83-R6 and (e,j) Co-Mo-S-0.83-Reac catalyst-modified graphite electrodes immersed into 0.10 M H<sub>2</sub>SO<sub>4</sub> aqueous electrolyte. Potential scan initiated at (A) 0.0 V in the positive direction or (B) +0.80 V in the negative direction; potential step increment 4 mV; square wave amplitude 25 mV; frequency 5 Hz.

The square wave voltammetry of the cathodic region ( $C_1$ ) also provided differences between the fresh and reused catalysts. As shown in Figure 8B, broad cathodic waves at +0.40 and -0.28 V are superimposed to peak signals at +0.32, +0.17, -0.06 and -0.40 V in the fresh catalyst. By comparison with the voltammogram of MoS<sub>2</sub> (Figure S16 in the Supporting Information), signals marked with asterisks at +0.32, +0.17, -0.06 V can be tentatively assigned to Mo(IV)-centered reduction processes to Mo(III) and Mo(II) sulfides successively. Interestingly, these signals are clearly diminished in the reused catalysts, thus denoting that the MoS<sub>2</sub> phase plays a role in the catalytic hydrogenation of **1a** and are partially consumed during the reaction. To our delight, the MoS<sub>2</sub> phase was found to be regenerated under the hydrothermal catalyst reactivation, as revealed by the enhancement of the signals at +0.32, +0.17, -0.06 V in catalysts Co-Mo-S-0.83-React.

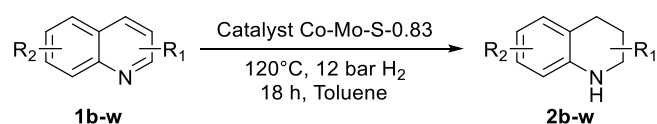
On the basis of all the above results we can conclude that the catalytic activity of these materials does not only depends on the composition of the mixed phase of cobalt sulfides, but also is associated with the presence of active, but poorly stable, Co-Mo-S structures that are mainly vanished after the first catalytic run.

### **Reaction Scope**

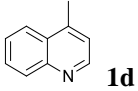
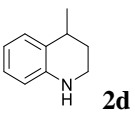
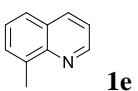
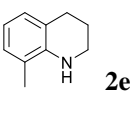
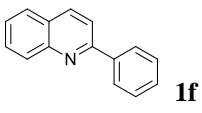
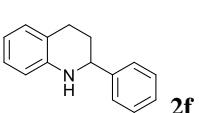
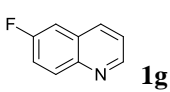
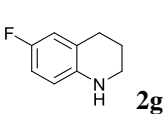
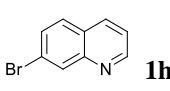
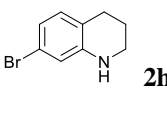
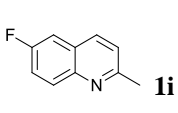
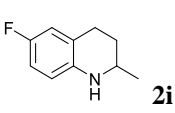
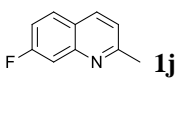
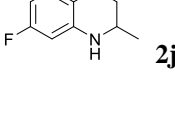
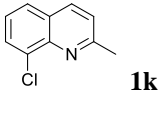
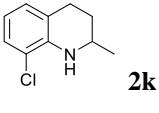
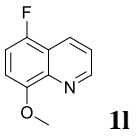
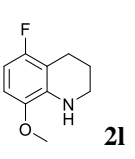
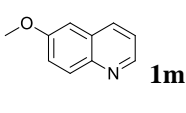
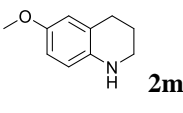
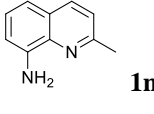
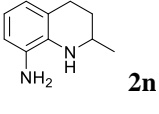
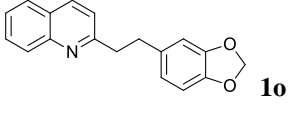
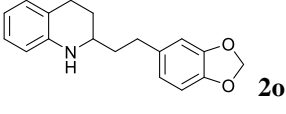
The scope of the chemo- and regioselective hydrogenation protocol in the presence of catalyst Co-Mo-S-0.83 was broadly investigated for the hydrogenation of a large number of quinolines substituted with different functional groups (Table 3). Notably, the catalytic process is completely regioselective towards the hydrogenation of the *N*-heteroarene ring to afford in all tested substrates the corresponding 1,2,3,4-tetrahydroquinolines, without formation of the corresponding 5,6,7,8-tetrahydro- or decahydro-derivatives. Quinolines **1b-1e** bearing a methyl group either on the benzene or the heteroarene ring reacted smoothly, affording the corresponding products in

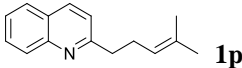
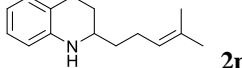
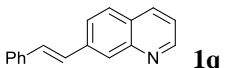
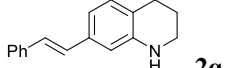
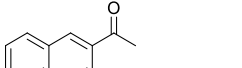
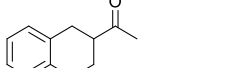
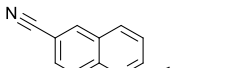
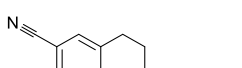
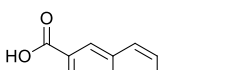
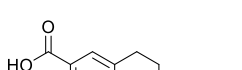
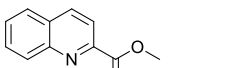
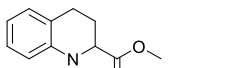
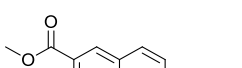
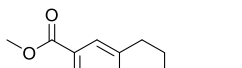
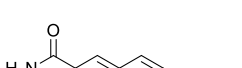
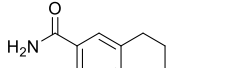
excellent yields (Table 3, entries 1-4). When the methyl group is located at the 4-position, higher temperature (150 °C) was required to get full conversion (Table 3, entry 3). In contrast, the more sterically hindered phenyl group at the 2-position had no significant influence on the activity of this catalytic system (Table 3, entry 5). Halogen-substituted quinolines were also readily transformed leading to the corresponding halogenated 1,2,3,4-tetrahydroquinolines **2g-2l** in high isolated yields (Table 3, entries 6-11). In this respect, the only exception is the hydrogenation of 7-bromoquinoline (**1h**) that required higher temperature (150 °C), higher catalyst loading and longer reaction time (24 h) to be fully converted (Table 3, entry 7). Under similar reaction conditions, 6-methoxyquinoline (**1m**) and 8-aminoquinoline (**1n**) were successfully hydrogenated to the desired products **2m** and **2n** in 90% and 85% isolated yield, respectively (Table 3, entries 12 and 13). Interestingly, this catalytic protocol was also applicable for the preparation, in excellent yield, of 2-(2-(benzo[*d*][1,3]-dioxol-5-yl)ethyl)-1,2,3,4-tetrahydroquinoline (**2o**), a direct precursor of the pharmacologically active natural product (±)-galipinine (Table 3, entry 14; see also Scheme S1 in the Supporting Information).<sup>37</sup>

**Table 3.** Chemo- and regioselective hydrogenation of substituted quinolines catalyzed by Co-Mo-S-0.83.<sup>a</sup>



Entry	Substrate	Product	Conv. (%) <sup>b</sup>	Yield (%) <sup>c</sup>
1			>99	96
2			>99	90

3 <sup>d</sup>	 <b>1d</b>	 <b>2d</b>	>99	91
4	 <b>1e</b>	 <b>2e</b>	>99	94
5	 <b>1f</b>	 <b>2f</b>	>99	96
6	 <b>1g</b>	 <b>2g</b>	>99	98
7 <sup>e,f,g</sup>	 <b>1h</b>	 <b>2h</b>	>99	50
8 <sup>h</sup>	 <b>1i</b>	 <b>2i</b>	>99	83
9	 <b>1j</b>	 <b>2j</b>	>99	92
10 <sup>i,j</sup>	 <b>1k</b>	 <b>2k</b>	>99	91
11	 <b>1l</b>	 <b>2l</b>	>99	95
12 <sup>f,k</sup>	 <b>1m</b>	 <b>2m</b>	96	90
13 <sup>f,k</sup>	 <b>1n</b>	 <b>2n</b>	98	85
14 <sup>f,l</sup>	 <b>1o</b>	 <b>2o</b>	>99	98

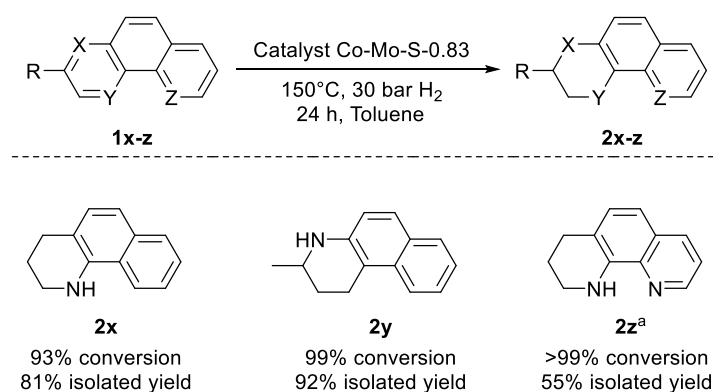
15 <sup>l,m</sup>			95	74
16 <sup>n</sup>			96	82
17 <sup>o,p</sup>			97	77
18 <sup>e,q,r</sup>			99	87
19 <sup>o,s</sup>			>99	74
20			>99	97
21 <sup>o</sup>			>99	96
22 <sup>f,k</sup>			98	78

<sup>a</sup>Reaction conditions: substrate (0.25 mmol), catalyst (6.5 mg), toluene (1.6 mL). <sup>b</sup>Determined by GC using dodecane as an internal standard. <sup>c</sup>yield of isolated product. <sup>d</sup>15 h, 150 °C. <sup>e</sup>18 h, 150 °C. <sup>f</sup>Catalyst (13.1 mg). <sup>g</sup>**2a** (15%) as by-product. <sup>h</sup>Traces (< 2%) of 1,2,3,4-Tetrahydroquinaldine as by-product. <sup>i</sup>18 h. <sup>j</sup>Traces (< 5%) of 1,2,3,4-Tetrahydroquinaldine as by-product. <sup>k</sup>24 h, 150 °C. <sup>l</sup>24 h. <sup>m</sup>Please, see Scheme S2 in the Supporting Information. <sup>n</sup>24 h, 110 °C, 30 bar H<sub>2</sub>; Traces (< 5%) of product with reduced double bond as by-product. <sup>o</sup>10 h, 150 °C. <sup>p</sup>3-ethyl-1,2,3,4-tetrahydroquinoline (15%) as by-product. <sup>q</sup>Catalyst (9.8 mg). <sup>r</sup>6-methyl-1,2,3,4-Tetrahydroquinoline (6%) and traces (< 2%) of 6-methylquinoline as by-products. <sup>s</sup>Traces (< 5%) of **2a** as by-product.

The functional group tolerance of this catalytic protocol was further studied by exploring other reducible substituents. Gratifyingly, high chemoselectivity to the *N*-heteroarene ring hydrogenation was achieved in the presence of sensitive alkene groups that were well-retained in the final hydrogenated products (Table 3, entries 15 and 16).

It should be noted that this selectivity is reached even at high conversions of substrates. Interestingly, the ketone sensitive group was also well tolerated under the hydrogenative reaction environment (Table 3, entry 17). Furthermore, 1,2,3,4-tetrahydroquinolines furnished with carboxylic acid derivative groups, including cyanides, acids, esters and amides (**2s-2w**) were also afforded in good to excellent isolated yields from their corresponding functionalized quinolines (Table 3, entries 18-22). To the best of our knowledge, the chemoselectivity in the presence of cyanide or amide functional groups have not been reported with homo- or heterogeneous catalysis.

Finally, we have further investigated the applicability of this catalytic protocol for the hydrogenation of other structurally related *N*-heteroarenes. As shown in Scheme 2, benzo[*h*]quinoline (**1x**) and 3-methylbenzo[*f*]quinoline (**1y**) were almost fully converted by hydrogenation of the *N*-heteroarene ring providing the corresponding products **2x** and **2y** in 81% and 92% isolated yields, respectively. Interestingly, for 1,10-phenanthroline (**1z**) only one *N*-heteroarene ring was hydrogenated obtaining 1,2,3,4-tetrahydro-1,10-phenanthroline (**2z**) in moderate yield.



**Scheme 2.** Regioselective hydrogenation of *N*-heteroarenes catalyzed by Co-Mo-S-0.83. Reaction conditions: substrate (0.25 mmol), catalyst (13.1 mg), toluene (1.6 mL).  
<sup>a</sup>20 bar H<sub>2</sub>.

## CONCLUSIONS

In summary, we have hydrothermally prepared a series of unsupported nanolayered cobalt-molybdenum sulfide based-materials with different chemical compositions that display abundance active sites per unit volume. All prepared catalysts exhibit good catalytic performance for the regioselective hydrogenation of the *N*-heteroarene ring of the quinoline. The most active catalyst (Co-Mo-S-0.83) presents a tunable phase composition constituted by MoS<sub>2</sub> and a mixed phase of cobalt sulfides, including CoS<sub>2</sub> and Co<sub>3</sub>S<sub>4</sub>. The electrochemical characterization has allowed us to detect transient species, likely associated to Co-Mo-S structures, which are mainly vanished after the first catalytic run. The superior activity of catalyst Co-Mo-S-0.83 could be attributed not only to the presence of these unstable Co-Mo-S structures, but also to the composition of the mixed phase of cobalt sulfides, being higher with the presence of Co<sub>3</sub>S<sub>4</sub> phase but lower when increasing the relative content of Co<sub>9</sub>S<sub>8</sub> phase. A catalyst phase transformation has been observed under successive catalyst reuses as a consequence of the vanishing of the ternary Co-Mo-S structures as well as to the catalyst desulfurization under hydrogenative conditions, thus leading to a variation of its catalytic performance. Recovering of most of the catalytic activity has been successfully accomplished by a facile hydrothermal re-sulfurization process that allows for regeneration of the mixed phase of cobalt sulfides and MoS<sub>2</sub>, but not the ternary Co-Mo-S structures.

Application of this non-noble metal-based heterogeneous catalyst has allowed for the efficient hydrogenation of functionalized quinolines and some other related *N*-heteroarenes to the corresponding tetrahydroderivatives. Notably, the catalyst displays high chemoselectivity for the hydrogenation of the *N*-heteroarene ring of the quinolines in the presence of other easily reducible groups, such as alkenes, ketones, cyanides,

carboxylic acids, esters and amides. This impressive chemoselectivity makes this catalyst unique in comparison with other heterogeneous catalytic protocols reported to date and extend the tool box of synthetic strategies for valuable *N*-heterocyclic compounds.

## EXPERIMENTAL SECTION

### **Synthesis of Co-Mo-S Catalysts**

The hydrothermal synthesis of unsupported Co-Mo-S catalysts was accomplished following the previously reported methodology used for the preparation of catalysts with lower or the same content of cobalt with respect to molybdenum (Co/(Mo + Co) mole ratio  $\leq 0.5$ ),<sup>29</sup> but different loading of Co(OAc)<sub>2</sub>·4H<sub>2</sub>O (471.6, 592.5, 1100.4 and 1650.7 mg) was used to obtain unsupported Co-Mo-S catalysts with Co/(Mo+Co) mole ratio  $> 0.5$  (0.58, 0.66, 0.83, 0.91, respectively).

### **Catalysts Characterization**

X-ray diffraction (XRD) patterns, electron microscopy (HRTEM and HAADF-STEM) images and textural properties (BET surface area, pore volume and pore diameter) of prepared Co-Mo-S catalysts were obtained as previously reported.<sup>29</sup>

Voltammetric measurements were performed in a conventional electrochemical cell using graphite bar (2 mm diameter) working electrodes, a Pt mesh auxiliary electrode and a Ag/AgCl (3 M NaCl) reference electrode using a CH I660 potentiostat. For voltammetry of immobilized particles (VIMP) experiments, the graphite electrode was modified by rubbing its lower end over ca. 1 mg of the Co-Mo-S material, previously grinded and finely distributed on the plane surface of an agate mortar. Then, the modified-graphite bar was rinsed with water to remove the ill-adhered particles and its lower end was immersed into the 0.10 M H<sub>2</sub>SO<sub>4</sub> aqueous electrolyte solution in the



electrochemical cell. This solution was optionally deaerated by bubbling Ar during 10 min. The voltammetric profiles of all measured materials were maintained in series of at least 10 successive measurements on the modified electrode.

### **Hydrogenation of Quinoline Derivatives**

The hydrogenation of quinoline derivatives was carried out in a 300 mL autoclave. Inside the autoclave, a 8 mL glass vial sealed with a perforated septum with a syringe needle, and containing a stirring bar, the Co-Mo-S catalyst (6.5 mg), the quinoline derivative (0.25 mmol), dodecane (50  $\mu$ L) as an internal standard and toluene (1.6 mL), was set in an alloy plate. Once the autoclave was tightly closed and purged 3 times with hydrogen up to 30 bar, it was pressurized to 12 bar and seated into an aluminum block located on a heating plate, which was set at 120 °C and 750 rpm of stirring speed. After reaction time, the autoclave was cooled down in an ice bath, and carefully depressurized. A sample of the reaction crude diluted with ethyl acetate was taken to be analyzed by GC. Reproducibility of these experiments was ensured by performing each reaction at least twice. The isolated yields of the tetrahydroderivative products were determine as follows: Catalytic reactions were carried in the absence of dodecane as an internal standard. After reaction time, ethyl acetate was added to the reaction mixture, which was filtered over celite and taken to dryness under reduced pressure. Prior to characterization, purification by silica gel chromatography was also accomplished for some of the products (see Supporting Information).

### **AUTHOR INFORMATION**

#### **Corresponding Author**

\*acorma@itq.upv.es

## Notes

The authors declare no competing financial interest.

## ASSOCIATED CONTENT

The Supporting Information is available free of charge via the Internet at

<http://pubs.acs.org>.

Extended morphological characterization of Co-Mo-S catalysts, details on preparation and characterization (XRD and HRTEM) of molybdenum-free cobalt sulfide catalysts Co-S-1 and Co-S-2, general procedure for the kinetic experiments, initial reaction rate depending on the stirring speed, additional reaction profiles for Co-Mo-S catalysts, comparison of catalytic activity per unit volume of catalyst, general procedure for the catalyst recycling experiments and catalyst reactivation, morphological characterization of reused and reactivated Co-Mo-S catalysts, catalyst recycling in the presence of H<sub>2</sub>S or sulfur, electrochemical characterization of reused and reactivated Co-Mo-S catalysts, experimental details for the catalytic hydrogenation of quinolines **1o**, **1p** and synthesis of **1q**, characterization data and experimental details of isolated tetrahydroderivative products

## ACKNOWLEDGMENT

Financial support by the Spanish Government-MINECO through program “Severo Ochoa” (SEV-2016-0683) is gratefully acknowledged. I.S. also thanks the Spanish Government-MINECO for a “Formación Postdoctoral” fellowship and Vice-Rectorate for Research, Innovation and Transfer of the Universitat Politècnica de València (UPV) for a postdoctoral fellowship. The authors also thank the Microscopy Service of UPV for kind help with TEM and STEM measurements.

## REFERENCES

- (1) (a) Topsoe, H.; Clausen, B. S.; Massoth, F. E. in *Hydrotreating Catalysis, Science and Technology*; Springer-Verlag: Heidelberg, 1996. (b) Toshiaki, K.; Atsushi, I.; Weihua, Q. in *Hydrodesulfurization and Hydrodenitrogenation: Chemistry and Engineering* Wiley-VCH: Tokyo, 1999. (c) Sánchez-Delgado, R. A. in *Organometallic Modeling of the Hydrodesulfurization and Hydrodenitrogenation Reactions*; Springer Netherlands: Kluwer, Dordrecht, 2002, p 1-34.
- (2) (a) Rylander, P. in *The Catalytic Hydrogenation in Organic Syntheses*; Academic Press Limited: London, 1979, p 213-234. (b) Nishimura, S. in *Handbook of Heterogeneous Catalytic Hydrogenations for Organic Synthesis*; John Wiley & Sons: New York, 2001, p 497-571. (c) Wang, D.-S.; Chen, Q.-A.; Lu, S.-M.; Zhou, Y.-G., Asymmetric Hydrogenation of Heteroarenes and Arenes. *Chem. Rev.* **2012**, *112*, 2557-2590.
- (3) (a) Katritzky, A. R.; Rachwal, S.; Rachwal, B., Recent Progress in the Synthesis of 1,2,3,4,-Tetrahydroquinolines. *Tetrahedron* **1996**, *52*, 15031-15070. (b) Scott, J. D.; Williams, R. M., Chemistry and Biology of the Tetrahydroisoquinoline Antitumor Antibiotics. *Chem. Rev.* **2002**, *102*, 1669-1730. (c) Sridharan, V.; Suryavanshi, P. A.; Menéndez, J. C., Advances in the Chemistry of Tetrahydroquinolines. *Chem. Rev.* **2011**, *111*, 7157-7259.
- (4) (a) Bird, C. W., Heteroaromaticity, 5, A Unified Aromaticity Index. *Tetrahedron* **1992**, *48*, 335-340. (b) Zhou, Y.-G., Asymmetric Hydrogenation of Heteroaromatic Compounds. *Acc. Chem. Res.* **2007**, *40*, 1357-1366.
- (5) (a) Sánchez-Delgado, R. A.; González, E., Selective Homogeneous Hydrogenation of Benzothiophene and Quinoline Catalysed by Ruthenium, Osmium,

Rhodium and Iridium Complexes. *Polyhedron* **1989**, *8*, 1431-1436. (b) Wang, W.-B.; Lu, S.-M.; Yang, P.-Y.; Han, X.-W.; Zhou, Y.-G., Highly Enantioselective Iridium-Catalyzed Hydrogenation of Heteroaromatic Compounds, Quinolines. *J. Am. Chem. Soc.* **2003**, *125*, 10536-10537. (c) Reetz, M. T.; Li, X., Asymmetric Hydrogenation of Quinolines Catalyzed by Iridium Complexes of BINOL-Derived Diphosphonites. *Chem. Commun.* **2006**, 2159-2160. (d) Qiu, L.; Kwong, F. Y.; Wu, J.; Lam, W. H.; Chan, S.; Yu, W.-Y.; Li, Y.-M.; Guo, R.; Zhou, Z.; Chan, A. S. C., A New Class of Versatile Chiral-Bridged Atropisomeric Diphosphine Ligands: Remarkably Efficient Ligand Syntheses and Their Applications in Highly Enantioselective Hydrogenation Reactions. *J. Am. Chem. Soc.* **2006**, *128*, 5955-5965. (e) Deport, C.; Buchotte, M.; Abecassis, K.; Tadaoka, H.; Ayad, T.; Ohshima, T.; Genet, J.-P.; Mashima, K.; Ratovelomanana-Vidal, V., Novel Ir-SYNPHOS® and Ir-DIFLUORPHOS® Catalysts for Asymmetric Hydrogenation of Quinolines. *Synlett* **2007**, 2743-2747. (f) Mršić, N.; Lefort, L.; Boogers, J. A. F.; Minnaard, A. J.; Feringa, B. L.; de Vries, J. G., Asymmetric Hydrogenation of Quinolines Catalyzed by Iridium Complexes of Monodentate BINOL-Derived Phosphoramidites. *Adv. Synth. Catal.* **2008**, *350*, 1081-1089. (g) Li, Z.-W.; Wang, T.-L.; He, Y.-M.; Wang, Z.-J.; Fan, Q.-H.; Pan, J.; Xu, L.-J., Air-Stable and Phosphine-Free Iridium Catalysts for Highly Enantioselective Hydrogenation of Quinoline Derivatives. *Org. Lett.* **2008**, *10*, 5265-5268. (h) Lu, S.-M.; Bolm, C., Synthesis of Sulfoximine-Derived P,N Ligands and their Applications in Asymmetric Quinoline Hydrogenations. *Adv. Synth. Catal.* **2008**, *350*, 1101-1105. (i) Yamaguchi, R.; Ikeda, C.; Takahashi, Y.; Fujita, K.-i., Homogeneous Catalytic System for Reversible Dehydrogenation–Hydrogenation Reactions of Nitrogen Heterocycles with Reversible Interconversion of Catalytic Species. *J. Am. Chem. Soc.* **2009**, *131*, 8410-8412. (j) Eggenstein, M.; Thomas, A.; Theuerkauf, J.; Franciò, G.; Leitner, W.,

Highly Efficient and Versatile Phosphine-Phosphoramidite Ligands for Asymmetric Hydrogenation. *Adv. Synth. Catal.* **2009**, *351*, 725-732. (k) Wang, D.-W.; Wang, X.-B.; Wang, D.-S.; Lu, S.-M.; Zhou, Y.-G.; Li, Y.-X., Highly Enantioselective Iridium-Catalyzed Hydrogenation of 2-Benzylquinolines and 2-Functionalized and 2,3-Disubstituted Quinolines. *J. Org. Chem.* **2009**, *74*, 2780-2787. (l) Tadaoka, H.; Cartigny, D.; Nagano, T.; Gosavi, T.; Ayad, T.; Genêt, J.-P.; Ohshima, T.; Ratovelomanana-Vidal, V.; Mashima, K., Unprecedented Halide Dependence on Catalytic Asymmetric Hydrogenation of 2-Aryl- and 2-Alkyl-Substituted Quolinium Salts by Using Ir Complexes with Difluorophos and Halide Ligands. *Chem. Eur. J.* **2009**, *15*, 9990-9994. (m) Dobereiner, G. E.; Nova, A.; Schley, N. D.; Hazari, N.; Miller, S. J.; Eisenstein, O.; Crabtree, R. H., Iridium-Catalyzed Hydrogenation of *N*-Heterocyclic Compounds under Mild Conditions by an Outer-Sphere Pathway. *J. Am. Chem. Soc.* **2011**, *133*, 7547-7562. (n) Wu, J.; Barnard, J. H.; Zhang, Y.; Talwar, D.; Robertson, C. M.; Xiao, J., Robust Cyclometallated Ir(III) Catalysts for the Homogeneous Hydrogenation of *N*-Heterocycles under Mild Conditions. *Chem. Commun.* **2013**, *49*, 7052-7054. (o) John, J.; Wilson-Konderka, C.; Metallinos, C., Low Pressure Asymmetric Hydrogenation of Quinolines using an Annulated Planar Chiral *N*-Ferrocenyl NHC-Iridium Complex. *Adv. Synth. Catal.* **2015**, *357*, 2071-2081. (p) Kuwano, R.; Hashiguchi, Y.; Ikeda, R.; Ishizuka, K., Catalytic Asymmetric Hydrogenation of Pyrimidines. *Angew. Chem. Int. Ed.* **2015**, *54*, 2393-2396.

(6) Fish, R. H.; Thormodsen, A. D.; Cremer, G. A., Homogeneous Catalytic Hydrogenation. 1. Regiospecific Reductions of Polynuclear Aromatic and Polynuclear Heteroaromatic Nitrogen Compounds Catalyzed by Transition Metal Carbonyl Hydrides. *J. Am. Chem. Soc.* **1982**, *104*, 5234-5237.

- (7) (a) Baralt, E.; Smith, S. J.; Hurwitz, J.; Horvath, I. T.; Fish, R. H., Homogeneous Catalytic Hydrogenation. 6. Synthetic and Mechanistic Aspects of the Regioselective Reductions of Model Coal Nitrogen, Sulfur, and Oxygen Heteroaromatic Compounds using the ( $\eta^5$ -Pentamethylcyclopentadienyl)rhodium Tris(acetonitrile) Dication Complex as the Catalyst Precursor. *J. Am. Chem. Soc.* **1992**, *114*, 5187-5196. (b) Rosales, M.; Bastidas, L. J.; González, B.; Vallejo, R.; Baricelli, P. J., Kinetics and Mechanisms of Homogeneous Catalytic Reactions. Part 11. Regioselective Hydrogenation of Quinoline Catalyzed by Rhodium Systems Containing 1,2-Bis(diphenylphosphino)ethane. *Catal. Lett.* **2011**, *141*, 1305-1310.
- (8) Zhu, G.; Pang, K.; Parkin, G., New Modes for Coordination of Aromatic Heterocyclic Nitrogen Compounds to Molybdenum: Catalytic Hydrogenation of Quinoline, Isoquinoline, and Quinoxaline by  $\text{Mo}(\text{PMe}_3)_4\text{H}_4$ . *J. Am. Chem. Soc.* **2008**, *130*, 1564-1565.
- (9) (a) Zhou, H.; Li, Z.; Wang, Z.; Wang, T.; Xu, L.; He, Y.; Fan, Q.-H.; Pan, J.; Gu, L.; Chan, A. S. C., Hydrogenation of Quinolines Using a Recyclable Phosphine-Free Chiral Cationic Ruthenium Catalyst: Enhancement of Catalyst Stability and Selectivity in an Ionic Liquid. *Angew. Chem. Int. Ed.* **2008**, *47*, 8464-8467. (b) Wang, T.; Zhuo, L.-G.; Li, Z.; Chen, F.; Ding, Z.; He, Y.; Fan, Q.-H.; Xiang, J.; Yu, Z.-X.; Chan, A. S. C., Highly Enantioselective Hydrogenation of Quinolines Using Phosphine-Free Chiral Cationic Ruthenium Catalysts: Scope, Mechanism, and Origin of Enantioselectivity. *J. Am. Chem. Soc.* **2011**, *133*, 9878-9891. (c) Kuwano, R.; Ikeda, R.; Hirasada, K., Catalytic Asymmetric Hydrogenation of Quinoline Carbocycles: Unusual Chemoselectivity in the Hydrogenation of Quinolines. *Chem. Commun.* **2015**, *51*, 7558-7561. (d) Ma, W.; Zhang, J.; Xu, C.; Chen, F.; He, Y.-M.; Fan, Q.-H., Highly Enantioselective Direct Synthesis of Endocyclic Vicinal Diamines through Chiral

Ru(diamine)-Catalyzed Hydrogenation of 2,2'-Bisquinoline Derivatives. *Angew. Chem. Int. Ed.* **2016**, *55*, 12891-12894.

(10) Chakraborty, S.; Brennessel, W. W.; Jones, W. D., A Molecular Iron Catalyst for the Acceptorless Dehydrogenation and Hydrogenation of *N*-Heterocycles. *J. Am. Chem. Soc.* **2014**, *136*, 8564-8567.

(11) Xu, R.; Chakraborty, S.; Yuan, H.; Jones, W. D., Acceptorless, Reversible Dehydrogenation and Hydrogenation of *N*-Heterocycles with a Cobalt Pincer Catalyst. *Acs Catal.* **2015**, *5*, 6350-6354. (b) Adam, R.; Cabrero-Antonino, J. R.; Spannenberg, A.; Junge, K.; Jackstell, R.; Beller, M., A General and Highly Selective Cobalt-Catalyzed Hydrogenation of *N*-Heteroarenes under Mild Reaction Conditions. *Angew. Chem. Int. Ed.* **2017**, *56*, 3216-3220.

(12) For an example on the use of a homogeneous Co-based catalyst for the transfer hydrogenation of quinolines, see: Cabrero-Antonino, J. R.; Adam, R.; Junge, K.; Jackstell, R.; Beller, M., Cobalt-Catalysed Transfer Hydrogenation of Quinolines and Related Heterocycles Using Formic Acid under Mild Conditions. *Catal. Sci. Technol.* **2017**, *7*, 1981-1985.

(13) (a) Norifumi, H.; Yusuke, T.; Takayoshi, H.; Shogo, S.; Takato, M.; Tomoo, M.; Koichiro, J.; Kiyotomi, K., Fine Tuning of Pd<sup>0</sup> Nanoparticle Formation on Hydroxyapatite and Its Application for Regioselective Quinoline Hydrogenation. *Chem. Lett.* **2010**, *39*, 832-834. (b) Gulyukina, N. S.; Beletskaya, I. P., Synthesis of 1-Hetarylethylphosphonates. *Russ. J. Org. Chem.* **2010**, *46*, 781-784. (c) Mao, H.; Chen, C.; Liao, X.; Shi, B., Catalytic Hydrogenation of Quinoline over Recyclable Palladium Nanoparticles Supported on Tannin Grafted Collagen Fibers. *J. Mol. Catal. A: Chem.* **2011**, *341*, 51-56. (d) Rahi, R.; Fang, M.; Ahmed, A.; Sanchez-Delgado, R. A.,

Hydrogenation of Quinolines, Alkenes, and Biodiesel by Palladium Nanoparticles Supported on Magnesium Oxide. *Dalton Trans.* **2012**, *41*, 14490-14497. (e) Gong, Y.; Zhang, P.; Xu, X.; Li, Y.; Li, H.; Wang, Y., A Novel Catalyst Pd@ompg-C<sub>3</sub>N<sub>4</sub> for Highly Chemoselective Hydrogenation of Quinoline under Mild Conditions. *J. Catal.* **2013**, *297*, 272-280. (f) Mao, H.; Ma, J.; Liao, Y.; Zhao, S.; Liao, X., Using Plant Tannin as Natural Amphiphilic Stabilizer to Construct an Aqueous-Organic Biphasic System for Highly Active and Selective Hydrogenation of Quinoline. *Catal. Sci. Technol.* **2013**, *3*, 1612-1617. (g) Dell'Anna, M. M.; Capodiferro, V. F.; Mali, M.; Manno, D.; Cotugno, P.; Monopoli, A.; Mastrorilli, P., Highly Selective Hydrogenation of Quinolines Promoted by Recyclable Polymer Supported Palladium Nanoparticles under Mild Conditions in Aqueous Medium. *Appl. Catal., A* **2014**, *481*, 89-95. (h) Zhang, S.; Xia, Z.; Ni, T.; Zhang, H.; Wu, C.; Qu, Y., Tuning Chemical Compositions of Bimetallic AuPd Catalysts for Selective Catalytic Hydrogenation of Halogenated Quinolines. *J. Mater. Chem. A* **2017**, *5*, 3260-3266. (i) Guo, M.; Li, C.; Yang, Q., Accelerated Catalytic Activity of Pd NPs Supported on Amine-Rich Silica Hollow Nanospheres for Quinoline Hydrogenation. *Catal. Sci. Technol.* **2017**, *7*, 2221-2227.

(14) (a) Beckers, N. A.; Huynh, S.; Zhang, X.; Luber, E. J.; Buriak, J. M., Screening of Heterogeneous Multimetallic Nanoparticle Catalysts Supported on Metal Oxides for Mono-, Poly-, and Heteroaromatic Hydrogenation Activity. *Acs Catal.* **2012**, *2*, 1524-1534. (b) Ge, D.; Hu, L.; Wang, J.; Li, X.; Qi, F.; Lu, J.; Cao, X.; Gu, H., Reversible Hydrogenation–Oxidative Dehydrogenation of Quinolines over a Highly Active Pt Nanowire Catalyst under Mild Conditions. *ChemCatChem* **2013**, *5*, 2183-2186. (c) Bai, L.; Wang, X.; Chen, Q.; Ye, Y.; Zheng, H.; Guo, J.; Yin, Y.; Gao, C., Explaining the Size Dependence in Platinum-Nanoparticle-Catalyzed Hydrogenation Reactions. *Angew. Chem. Int. Ed.* **2016**, *55*, 15656-15661.



(15) (a) Campanati, M.; Casagrande, M.; Fagiolino, I.; Lenarda, M.; Storaro, L.; Battagliarin, M.; Vaccari, A., Mild Hydrogenation of Quinoline. *J. Mol. Catal. A: Chem.* **2002**, *184*, 267-272. (b) Campanati, M.; Vaccari, A.; Piccolo, O., Mild Hydrogenation of Quinoline. *J. Mol. Catal. A: Chem.* **2002**, *179*, 287-292. (c) Mévellec, V.; Roucoux, A., Nanoheterogeneous Catalytic Hydrogenation of N-, O- or S-Heteroaromatic Compounds by Re-Usable Aqueous Colloidal Suspensions of Rhodium(0). *Inorg. Chim. Acta* **2004**, *357*, 3099-3103. (d) Zhandarev, V. V.; Goshin, M. E.; Kazin, V. N.; Ramenskaya, L. M.; Mironov, G. S.; Shishkina, A. L., Catalytic Synthesis of New Halogen-Containing Tetrahydroquinolin-8-ols. *Russ. J. Org. Chem.* **2006**, *42*, 1093-1094. (e) Fan, G.-Y.; Wu, J., Mild Hydrogenation of Quinoline to Decahydroquinoline over Rhodium Nanoparticles Entrapped in Aluminum Oxy-Hydroxide. *Catal. Commun.* **2013**, *31*, 81-85. (f) Sánchez, A.; Fang, M.; Ahmed, A.; Sánchez-Delgado, R. A., Hydrogenation of Arenes, N-heteroaromatic Compounds, and Alkenes Catalyzed by Rhodium Nanoparticles Supported on Magnesium Oxide. *Appl. Catal., A* **2014**, *477*, 117-124. (g) Niu, M.; Wang, Y.; Chen, P.; Du, D.; Jiang, J.; Jin, Z., Highly Efficient and Recyclable Rhodium Nanoparticle Catalysts for Hydrogenation of Quinoline and Its Derivatives. *Catal. Sci. Technol.* **2015**, *5*, 4746-4749. (h) Jiang, H.-Y.; Zheng, X.-X., Phosphine-Functionalized Ionic Liquid-Stabilized Rhodium Nanoparticles for Selective Hydrogenation of Aromatic Compounds. *Appl. Catal., A* **2015**, *499*, 118-123. (i) Karakulina, A.; Gopakumar, A.; Akçok, İ.; Roulier, B. L.; LaGrange, T.; Katsyuba, S. A.; Das, S.; Dyson, P. J., A Rhodium Nanoparticle–Lewis Acidic Ionic Liquid Catalyst for the Chemoselective Reduction of Heteroarenes. *Angew. Chem. Int. Ed.* **2016**, *55*, 292-296.

(16) (a) Bianchini, C.; Dal Santo, V.; Meli, A.; Moneti, S.; Moreno, M.; Oberhauser, W.; Psaro, R.; Sordelli, L.; Vizza, F., A Comparison between Silica-Immobilized

Ruthenium(II) Single Sites and Silica-Supported Ruthenium Nanoparticles in the Catalytic Hydrogenation of Model Hetero- and Polyaromatics Contained in Raw Oil Materials. *J. Catal.* **2003**, *213*, 47-62. (b) Sánchez-Delgado, R. A.; Machalaba, N.; Ng-a-qui, N., Hydrogenation of Quinoline by Ruthenium Nanoparticles Immobilized on Poly(4-vinylpyridine). *Catal. Commun.* **2007**, *8*, 2115-2118. (c) Sun, Y.-P.; Fu, H.-Y.; Zhang, D.-l.; Li, R.-X.; Chen, H.; Li, X.-J., Complete Hydrogenation of Quinoline over Hydroxyapatite Supported Ruthenium Catalyst. *Catal. Commun.* **2010**, *12*, 188-192. (d) Fang, M.; Machalaba, N.; Sanchez-Delgado, R. A., Hydrogenation of Arenes and *N*-Heteroaromatic Compounds over Ruthenium Nanoparticles on Poly(4-vinylpyridine): A Versatile Catalyst Operating by a Substrate-Dependent Dual Site Mechanism. *Dalton Trans.* **2011**, *40*, 10621-10632. (e) Sun, B.; Khan, F.-A.; Vallat, A.; Süß-Fink, G., NanoRu@hectorite: A Heterogeneous Catalyst with Switchable Selectivity for the Hydrogenation of Quinoline. *Appl. Catal., A* **2013**, *467*, 310-314. (f) Fang, M.; Sánchez-Delgado, R. A., Ruthenium Nanoparticles Supported on Magnesium Oxide: A Versatile and Recyclable Dual-Site Catalyst for Hydrogenation of Mono- and Poly-Cyclic Arenes, *N*-Heteroaromatics, and *S*-Heteroaromatics. *J. Catal.* **2014**, *311*, 357-368. (g) Zhang, L.; Wang, X.; Xue, Y.; Zeng, X.; Chen, H.; Li, R.; Wang, S., Cooperation between the Surface Hydroxyl Groups of Ru-SiO<sub>2</sub>@mSiO<sub>2</sub> and Water for Good Catalytic Performance for Hydrogenation of Quinoline. *Catal. Sci. Technol.* **2014**, *4*, 1939-1948. (h) Jiang, H.-Y.; Zheng, X.-X., Tuning the Chemoselective Hydrogenation of Aromatic Ketones, Aromatic Aldehydes and Quinolines Catalyzed by Phosphine Functionalized Ionic Liquid Stabilized Ruthenium Nanoparticles. *Catal. Sci. Technol.* **2015**, *5*, 3728-3734. (i) Tang, M.; Deng, J.; Li, M.; Li, X.; Li, H.; Chen, Z.; Wang, Y., 3D-Interconnected Hierarchical Porous *N*-Doped Carbon Supported Ruthenium Nanoparticles as an Efficient Catalyst for Toluene and Quinoline

Hydrogenation. *Green Chem.* **2016**, *18*, 6082-6090. (j) Chen, Y.; Yu, Z.; Chen, Z.; Shen, R.; Wang, Y.; Cao, X.; Peng, Q.; Li, Y., Controlled One-Pot Synthesis of RuCu Nanocages and Cu@Ru Nanocrystals for the Regioselective Hydrogenation of Quinoline. *Nano Res.* **2016**, *9*, 2632-2640. (k) Ye, T.-N.; Li, J.; Kitano, M.; Hosono, H., Unique Nanocages of  $12\text{CaO}\cdot 7\text{Al}_2\text{O}_3$  Boost Heterolytic Hydrogen Activation and Selective Hydrogenation of Heteroarenes over Ruthenium Catalyst. *Green Chem.* **2017**, *19* (3), 749-756. (l) Konnerth, H.; Prechtel, M. H. G., Selective Hydrogenation of *N*-Heterocyclic Compounds using Ru Nanocatalysts in Ionic Liquids. *Green Chem.* **2017**, *19*, 2762-2767.

(17) (a) Barbaro, P.; Gonsalvi, L.; Guerriero, A.; Liguori, F., Facile Heterogeneous Catalytic Hydrogenations of C=N and C=O Bonds in Neat Water: Anchoring of Water-Soluble Metal Complexes onto Ion-Exchange Resins. *Green Chem.* **2012**, *14*, 3211-3219. (b) Ji, Y.-G.; Wei, K.; Liu, T.; Wu, L.; Zhang, W.-H., "Naked" Iridium(IV) Oxide Nanoparticles as Expedient and Robust Catalysts for Hydrogenation of Nitrogen Heterocycles: Remarkable Vicinal Substitution Effect and Recyclability. *Adv. Synth. Catal.* **2017**, *359*, 933-940.

(18) Ren, D.; He, L.; Yu, L.; Ding, R. S.; Liu, Y. M.; Cao, Y.; He, H. Y.; Fan, K. N., An Unusual Chemoselective Hydrogenation of Quinoline Compounds Using Supported Gold Catalysts. *J. Am. Chem. Soc.* **2012**, *134*, 17592-17598.

(19) For examples on the Au-catalyzed chemoselective hydrogenation of quinolines in the presence of double bonds using silanes or formic acid as reducing agents, see respectively: (a) Yan, M.; Jin, T.; Chen, Q.; Ho, H. E.; Fujita, T.; Chen, L.-Y.; Bao, M.; Chen, M.-W.; Asao, N.; Yamamoto, Y., Unsupported Nanoporous Gold Catalyst for Highly Selective Hydrogenation of Quinolines. *Org. Lett.* **2013**, *15*, 1484-1487. (b) Tao,

L.; Zhang, Q.; Li, S.-S.; Liu, X.; Liu, Y.-M.; Cao, Y., Heterogeneous Gold-Catalyzed Selective Reductive Transformation of Quinolines with Formic Acid. *Adv. Synth. Catal.* **2015**, *357*, 753-760.

(20) (a) Hiroshi, O.; Kiyotaka, O.; Mahito, S.; Yoshio, I.; Ryuji, T.; Isao, M., Hydrogenation Pathway of Quinolines over Raney Nickel and Ru/C. *Bull. Chem. Soc. Jpn.* **1990**, *63*, 3167-3174. (b) Czaplik, W. M.; Neudorfl, J.-M.; von Wangelin, A. J., On the Quantitative Recycling of Raney-Nickel Catalysts on a Lab-Scale. *Green Chem.* **2007**, *9*, 1163-1165.

(21) (a) Chen, F.; Surkus, A.-E.; He, L.; Pohl, M.-M.; Radnik, J.; Topf, C.; Junge, K.; Beller, M., Selective Catalytic Hydrogenation of Heteroarenes with *N*-Graphene-Modified Cobalt Nanoparticles (Co<sub>3</sub>O<sub>4</sub>-Co/NGr@ $\alpha$ -Al<sub>2</sub>O<sub>3</sub>). *J. Am. Chem. Soc.* **2015**, *137*, 11718-11724. (b) Wei, Z.; Chen, Y.; Wang, J.; Su, D.; Tang, M.; Mao, S.; Wang, Y., Cobalt Encapsulated in *N*-Doped Graphene Layers: An Efficient and Stable Catalyst for Hydrogenation of Quinoline Compounds. *Acs Catal.* **2016**, *6*, 5816-5822. (c) Ji, P.; Manna, K.; Lin, Z.; Urban, A.; Greene, F. X.; Lan, G.; Lin, W., Single-Site Cobalt Catalysts at New Zr<sub>8</sub>( $\mu_2$ -O)<sub>8</sub>( $\mu_2$ -OH)<sub>4</sub> Metal-Organic Framework Nodes for Highly Active Hydrogenation of Alkenes, Imines, Carbonyls, and Heterocycles. *J. Am. Chem. Soc.* **2016**, *138*, 12234-12242.

(22) For an example on the use of a family related catalyst for the transfer hydrogenation of *N*-heteroarenes, see: Chen, F.; Sahoo, B.; Kreyenschulte, C.; Lund, H.; Zeng, M.; He, L.; Junge, K.; Beller, M., Selective Cobalt Nanoparticles for Catalytic Transfer Hydrogenation of *N*-Heteroarenes. *Chem. Sci.* **2017**, *8*, 6239-6246.

(23) (a) Cocchetto, J. F.; Satterfield, C. N., Chemical Equilibria among Quinoline and Its Reaction Products in Hydrodenitrogenation. *Ind. Eng. Chem. Process Des. Dev.*

**1981**, 20, 49-53. (b) Satterfield, C. N.; Cocchetto, J. F., Reaction Network and Kinetics of the Vapor Phase Catalytic Hydrodenitrogenation of Quinoline. *Ind. Eng. Chem. Process Des. Dev.* **1981**, 20, 53-62. (c) Perot, G., The Reactions Involved in Hydrodenitrogenation. *Catal. Today* **1991**, 10, 447-472. (d) Prins, R. in *Advances in Catalysis*; Academic Press: 2001; Vol. 46, p 399-464.

(24) (a) Curtis, C. W.; Cahela, D. R., Hydrodenitrogenation of Quinoline and Coal using Precipitated Transition-Metal Sulfides. *Energy & Fuels* **1989**, 3, 168-174. (b) Callant, M.; Grange, P.; Holder, K. A.; Viehe, H. G.; Delmon, B., Secondary Effects in Catalytic Tests for Hydrodenitrogenation Reactions Due to Side Reactions with Sulfur Compounds. *J. Catal.* **1993**, 142, 725-728. (c) Callant, M.; Holder, K. A.; Viehe, H. G.; Grange, P.; Delmon, B., Methylation of Indole during Catalytic Tests for Hydrodenitrogenation (HDN) Reactions. *J. Mol. Catal. A: Chem.* **1995**, 97, 57-64. (d) Yang, M.-H.; Grange, P.; Delmon, B., Secondary Effect of Hydrogen Sulfide on HDN Reaction. *Appl. Catal., A* **1997**, 154, L7-L15. (e) Eijsbouts, S.; Mayo, S. W.; Fujita, K., Unsupported Transition Metal Sulfide Catalysts: From Fundamentals to Industrial Application. *Appl. Catal., A* **2007**, 322, 58-66.

(25) (a) Topsoe, H.; Clausen, B. S.; Candia, R.; Wivel, C.; Morup, S., *In Situ* Mössbauer Emission Spectroscopy Studies of Unsupported and Supported Sulfided Co-Mo Hydrodesulfurization Catalysts: Evidence for and Nature of a Co-Mo-S Phase. *J. Catal.* **1981**, 68, 433-452. (b) Wivel, C.; Candia, R.; Clausen, B. S.; Morup, S.; Topsoe, H., On the catalytic significance of a Co-Mo-S phase in Co-Mo/Al<sub>2</sub>O<sub>3</sub> Hydrodesulfurization Catalysts: Combined *In Situ* Mössbauer Emission Spectroscopy and Activity Studies. *J. Catal.* **1981**, 68, 453-463. (c) Clausen, B. S.; Topsoe, H.; Candia, R.; Villadsen, J.; Lengeler, B.; Alsniesen, J.; Christensen, F., Extended X-Ray Absorption Fine-Structure Study of Co-Mo Hydrodesulfurization Catalysts. *J. Phys.*

*Chem.* **1981**, *85*, 3868-3872. (d) Breysse, M.; Bennett, B. A.; Chadwick, D.; Vrinat, M., Structure and HDS Activity of Co-Mo Catalysts – A Comparison of Alumina and Carbon Supports. *Bull. Soc. Chim. Belg.* **1981**, *90*, 1271-1277. (e) Topsoe, N. Y.; Topsoe, H., Characterization of the Structures and Active-Sites in Sulfided Co-Mo/Al<sub>2</sub>O<sub>3</sub> and Ni-Mo/Al<sub>2</sub>O<sub>3</sub> Catalysts by NO Chemisorption. *J. Catal.* **1983**, *84*, 386-401. (f) Kasztelan, S.; Toulhoat, H.; Grimblot, J.; Bonnelle, J. P., A Geometrical Model of the Active Phase of Hydrotreating Catalysts. *Appl. Catal.* **1984**, *13*, 127-159. (g) Topsøe, H.; Clausen, B. S., Active Sites and Support Effects in Hydrodesulfurization Catalysts. *Appl. Catal.* **1986**, *25*, 273-293. (h) Byskov, L. S.; Nørskov, J. K.; Clausen, B. S.; Topsøe, H., DFT Calculations of Unpromoted and Promoted MoS<sub>2</sub>-Based Hydrodesulfurization Catalysts. *J. Catal.* **1999**, *187*, 109-122. (i) Schweiger, H.; Raybaud, P.; Toulhoat, H., Promoter Sensitive Shapes of Co(Ni)MoS Nanocatalysts in Sulfo-Reductive Conditions. *J. Catal.* **2002**, *212*, 33-38. (j) Lauritsen, J. V.; Bollinger, M. V.; Lægsgaard, E.; Jacobsen, K. W.; Nørskov, J. K.; Clausen, B. S.; Topsøe, H.; Besenbacher, F., Atomic-Scale Insight into Structure and Morphology Changes of MoS<sub>2</sub> Nanoclusters in Hydrotreating Catalysts. *J. Catal.* **2004**, *221*, 510-522. (k) Topsoe, H., The Role of Co-Mo-S Type Structures in Hydrotreating Catalysts. *Appl. Catal., A* **2007**, *322*, 3-8. (l) Lauritsen, J. V.; Kibsgaard, J.; Olesen, G. H.; Moses, P. G.; Hinnemann, B.; Helveg, S.; Nørskov, J. K.; Clausen, B. S.; Topsøe, H.; Lægsgaard, E.; Besenbacher, F., Location and Coordination of Promoter Atoms in Co- and Ni-Promoted MoS<sub>2</sub>-Based Hydrotreating Catalysts. *J. Catal.* **2007**, *249*, 220-233. (m) Berhault, G.; Perez De la Rosa, M.; Mehta, A.; Yácaman, M. J.; Chianelli, R. R., The Single-Layered Morphology of Supported MoS<sub>2</sub>-Based Catalysts—The Role of the Cobalt Promoter and Its Effects in the Hydrodesulfurization of Dibenzothiophene. *Appl. Catal., A* **2008**, *345*, 80-88. (n) Besenbacher, F.; Brorson, M.; Clausen, B. S.; Helveg, S.; Hinnemann,

B.; Kibsgaard, J.; Lauritsen, J. V.; Moses, P. G.; Nørskov, J. K.; Topsøe, H., Recent STM, DFT and HAADF-STEM Studies of Sulfide-Based Hydrotreating Catalysts: Insight into Mechanistic, Structural and Particle Size Effects. *Catal. Today* **2008**, *130*, 86-96. (o) Gandubert, A. D.; Krebs, E.; Legens, C.; Costa, D.; Guillaume, D.; Raybaud, P., Optimal Promoter Edge Decoration of CoMoS Catalysts: A Combined Theoretical and Experimental Study. *Catal. Today* **2008**, *130*, 149-159. (p) Krebs, E.; Silvi, B.; Raybaud, P., Mixed Sites and Promoter Segregation: A DFT Study of the Manifestation of Le Chatelier's Principle for the Co(Ni)MoS Active Phase in Reaction Conditions. *Catal. Today* **2008**, *130*, 160-169. (q) Kibsgaard, J.; Tuxen, A.; Knudsen, K. G.; Brorson, M.; Topsøe, H.; Lægsgaard, E.; Lauritsen, J. V.; Besenbacher, F., Comparative Atomic-Scale Analysis of Promotional Effects by Late 3d-Transition Metals in MoS<sub>2</sub> Hydrotreating Catalysts. *J. Catal.* **2010**, *272*, 195-203. (r) Zhu, Y.; Ramasse, Q. M.; Brorson, M.; Moses, P. G.; Hansen, L. P.; Kisielowski, C. F.; Helveg, S., Visualizing the Stoichiometry of Industrial-Style Co-Mo-S Catalysts with Single-Atom Sensitivity. *Angew. Chem. Int. Ed.* **2014**, *53*, 10723-10727.

(26) For reports that explain the catalytic activity of these materials by the Remote Control model through a migration of hydrogen spillover between sulfide phases, see: (a) Delmon, B., New Mechanistic Model Explaining Synergy in Hydrotreating Catalysts. *C. R. Hebd. Séances Acad. Sci. Serie C* **1979**, *289*, 173-176. (b) Delmon, B., A New Hypothesis Explaining Synergy between 2 Phases in Heterogeneous Catalysis – Case of Hydrodesulfurization Catalysts. *Bull. Soc. Chim. Belg.* **1979**, *88*, 979-987. (c) Karroua, M.; Grange, P.; Delmon, B., Existence of Synergy between “CoMoS” and Co<sub>9</sub>S<sub>8</sub>: New Proof of Remote Control in Hydrodesulfurization. *Appl. Catal.* **1989**, *50*, L5-L10. (d) Delmon, B., Selectivity in HDS, HDN, HDO and Hydrocracking Contribution of Remote Control and Other New Concepts. *Bull. Soc. Chim. Belg.* **1995**,

104, 173-187. (e) Stumbo, A. M.; Grange, P.; Delmon, B., Spillover Hydrogen Effect on Amorphous Hydrocracking Catalysts. *Catal. Lett.* **1995**, *31*, 173-182. (f) Mohamed, K.; Haris, M.; Edgardo, S.; Paul, G.; Bernard, D., Synergy between the CoMoS Phase and Supported or Unsupported Cobalt Sulfide. Existence of a Remote Control Effect. *Bull. Chem. Soc. Jpn.* **1995**, *68*, 107-119. (g) Delmon, B.; Froment, G. F., Remote Control of Catalytic Sites by Spillover Species: A Chemical Reaction Engineering Approach. *Cat. Rev. - Sci. Eng.* **1996**, *38*, 69-100. (h) Li, Y. W.; Delmon, B., Modelling of Hydrotreating Catalysis Based on the Remote Control: HYD and HDS. *J. Mol. Catal. A: Chem.* **1997**, *127*, 163-190. (i) Baeza, P.; Ureta-Zañartu, M. S.; Escalona, N.; Ojeda, J.; Gil-Llambías, F. J.; Delmon, B., Migration of Surface Species on Supports: A Proof of Their Role on the Synergism between CoS<sub>x</sub> or NiS<sub>x</sub> and MoS<sub>2</sub> in HDS. *Appl. Catal., A* **2004**, *274*, 303-309. (j) Baeza, P.; Villarroel, M.; Ávila, P.; López Agudo, A.; Delmon, B.; Gil-Llambías, F. J., Spillover Hydrogen Mobility during Co–Mo Catalyzed HDS in Industrial-Like Conditions. *Appl. Catal., A* **2006**, *304*, 109-115. (k) Villarroel, M.; Baeza, P.; Escalona, N.; Ojeda, J.; Delmon, B.; Gil-Llambías, F. J., MD//Mo and MD//W [MD=Mn, Fe, Co, Ni, Cu and Zn] Promotion Via Spillover Hydrogen in Hydrodesulfurization. *Appl. Catal., A* **2008**, *345*, 152-157.

(27) (a) Rangarajan, S.; Mavrikakis, M., DFT Insights into the Competitive Adsorption of Sulfur- and Nitrogen-Containing Compounds and Hydrocarbons on Co-Promoted Molybdenum Sulfide Catalysts. *Acs Catal.* **2016**, *6*, 2904-2917. (b) Berit, H.; Poul Georg, M.; Jens, K. N., Recent Density Functional Studies of Hydrodesulfurization Catalysts: Insight into Structure and Mechanism. *J. Phys.: Condens. Matter* **2008**, *20*, 064236. (c) Temel, B.; Tuxen, A. K.; Kibsgaard, J.; Topsøe, N.-Y.; Hinnemann, B.; Knudsen, K. G.; Topsøe, H.; Lauritsen, J. V.; Besenbacher, F., Atomic-Scale Insight



into the Origin of Pyridine Inhibition of MoS<sub>2</sub>-Based Hydrotreating Catalysts. *J. Catal.* **2010**, *271*, 280-289.

(28) For examples on the hydrogenation of quinolines with transition metal sulfides, see: (a) Shaw, J. E.; Stapp, P. R., Regiospecific Hydrogenation of Quinolines and Indoles in the Heterocyclic Ring. *J. Heterocycl. Chem.* **1987**, *24*, 1477-1483. (b) Ma, C.; Jin, X.; Ding, L.; Mang, Q.; Qiu, J.; Liang, C., Preparation of High-Surface-Area MoS<sub>2</sub> and Its Catalytic Performance for Selective Hydrogenation of Quinoline. *Chin. J. Catal.* **2009**, *30*, 78-82.

(29) Sorribes, I.; Liu, L.; Corma, A., Nanolayered Co-Mo-S Catalysts for the Chemoselective Hydrogenation of Nitroarenes. *Acs Catal.* **2017**, *7*, 2698-2708.

(30) Wang, W.; Zhang, K.; Li, L.; Wu, K.; Liu, P.; Yang, Y., Synthesis of Highly Active Co-Mo-S Unsupported Catalysts by a One-Step Hydrothermal Method for p-Cresol Hydrodeoxygenation. *Ind. Eng. Chem. Res.* **2014**, *53*, 19001-19009.

(31) (a) Park, S.-K.; Yu, S.-H.; Woo, S.; Ha, J.; Shin, J.; Sung, Y.-E.; Piao, Y., A Facile and Green Strategy for the Synthesis of MoS<sub>2</sub> Nanospheres with Excellent Li-Ion Storage Properties. *CrystEngComm* **2012**, *14*, 8323-8325. (b) Wang, Z.; Chen, T.; Chen, W.; Chang, K.; Ma, L.; Huang, G.; Chen, D.; Lee, J. Y., CTAB-Assisted Synthesis of Single-Layer MoS<sub>2</sub>-Graphene Composites as Anode Materials of Li-Ion Batteries. *J. Mater. Chem. A* **2013**, *1*, 2202-2210.

(32) (a) Soled, S. L.; Miseo, S.; Krycak, R.; Vroman, H.; Ho, T. C.; Riley, K. U. S. Patent 6,299,760 to Exxonmobil, 2001. (b) Plantenga, F. L.; Cerfontain, R.; Eijssbouts, S.; van Houtert, F.; Anderson, G. H.; Miseo, S.; Soled, S.; Riley, K.; Fujita, K.; Inoue,

Y. In *Stud. Surf. Sci. Catal.*; Anpo, M., Onaka, M., Yamashita, H., Eds.; Elsevier: 2003; Vol. Volume 145, p 407-410.

(33) Rosenqvist, T., A Thermodynamic Study of the Iron, Cobalt, and Nickel Sulphides. *J. Iron Steel Inst., London* **1954**, *176*, 37-57.

(34) Scholz, F.; Schröder, U.; Gulaboski, R.; Doménech-Carbó, A. in *Electrochemistry of Immobilized Particles and Droplets*; 2<sup>nd</sup> ed.; Springer: Berlin-Heidelberg, 2014.

(35) Domenech-Carbo, A.; Labuda, J.; Scholz, F., Electroanalytical Chemistry for the Analysis of Solids: Characterization and Classification (IUPAC Technical Report). *Pure Appl. Chem.* **2013**, *85*, 609-631.

(36) (a) Sun, Y.; Liu, C.; Grauer, D. C.; Yano, J.; Long, J. R.; Yang, P.; Chang, C. J., Electrodeposited Cobalt-Sulfide Catalyst for Electrochemical and Photoelectrochemical Hydrogen Generation from Water. *J. Am. Chem. Soc.* **2013**, *135*, 17699-17702. (b) Gao, M.-R.; Liang, J.-X.; Zheng, Y.-R.; Xu, Y.-F.; Jiang, J.; Gao, Q.; Li, J.; Yu, S.-H., An efficient Molybdenum Disulfide/Cobalt Diselenide Hybrid Catalyst for Electrochemical Hydrogen Generation. *Nat. Commun.* **2015**, *6*, 5982.

(37) (a) Houghton, P. J.; Woldemariam, T. Z.; Watanabe, Y.; Yates, M., Activity Against Mycobacterium Tuberculosis of Alkaloid Constituents of Angostura Bark, Galipea Officinalis. *Planta Med* **1999**, *65*, 250-254. (b) Jacquemond-Collet, I.; Benoit-Vical, F.; Valentin, M.; Stanislas, A.; Mallié, E.; Fourasté, M.; Isabelle, Antiplasmodial and Cytotoxic Activity of Galipinine and other Tetrahydroquinolines from Galipea Officinalis. *Planta Med* **2002**, *68*, 68-69.

TABLE OF CONTENTS ARTWORK

